Journal of Inorganic Biochemistry 249 (2023) 112391

Contents lists available at ScienceDirect

Journal of Inorganic Biochemistry

journal homepage: www.elsevier.com/locate/jinorgbio

Characterisation of the heme aqua-ligand coordination environment in an engineered peroxygenase cytochrome P450 variant

Matthew N. Podgorski [a], Joel H.Z. Lee [a], Joshua S. Harbort [b], Giang T.H. Nguyen [c], Daniel Z. Doherty [a], William A. Donald [c], Jeffrey R. Harmer [b], John B. Bruning [d], Stephen G. Bell [a,*]

[a] Department of Chemistry, University of Adelaide, Adelaide, SA 5005, Australia
[b] Australian Institute for Bioengineering and Nanotechnology, University of Queensland, St Lucia, QLD 4072, Australia
[c] School of Chemistry, University of New South Wales, Sydney, New South Wales 2052, Australia
[d] School of Biological Sciences, University of Adelaide, SA 5005, Australia

ARTICLE INFO

Keywords:
Heme enzymes
Peroxygenases
Protein engineering
Dioxygen activation
X-ray crystallography
Metalloenzymes

ABSTRACT

The cytochrome P450 enzymes (CYPs) are heme-thiolate monooxygenases that catalyse the insertion of an oxygen atom into the C–H bonds of organic molecules. In most CYPs, the activation of dioxygen by the heme is aided by an acid-alcohol pair of residues located in the I-helix of the enzyme. Mutation of the threonine residue of this acid-alcohol pair of CYP199A4, from the bacterium *Rhodospeudomonas palustris* HaA2, to a glutamate residue induces peroxygenase activity. In the X-ray crystal structures of this variant an interaction of the glutamate side chain and the distal aqua ligand of the heme was observed and this results in this ligand not being readily displaced in the peroxygenase mutant on the addition of substrate. Here we use a range of bulky hydrophobic and nitrogen donor containing ligands in an attempt to displace the distal aqua ligand of the T252E mutant of CYP199A4. Ligand binding was assessed by UV–visible absorbance spectroscopy, native mass spectrometry, electron paramagnetic resonance and X-ray crystallography. None of the ligands tested, even the nitrogen donor ligands which bind directly to the iron in the wild-type enzyme, resulted in displacement of the aqua ligand. Therefore, modification of the I-helix threonine residue to a glutamate residue results in a significant strengthening of the ferric distal aqua ligand. This ligand was not displaced using any of the ligands during this study and this provides a rationale as to why this mutant can shutdown the monooxygenase pathway of this enzyme and switch to peroxygenase activity.

1. Introduction

The cytochrome P450 enzymes (CYPs) are heme-thiolate monooxygenases whose predominant role is to insert an oxygen atom into C–H bonds. [1] They do this by using dioxygen which is activated by the heme-thiolate system after sourcing two electrons (from nicotinamide cofactors) and two protons. [2] In excess of one million P450s have been discovered across all kingdoms of life including archaea, fungi, bacteria, animals, plants and even viruses. [3–5] The P450 superfamily is exceptionally versatile and its members can catalyse a range of other oxidation and reduction reactions including epoxidation, desaturation, dealkylation, heteroatom oxidations and C–C bond formation. [6–8] They can be modified to perform unnatural reactions such as cyclopropanation and amination. [9–12] Therefore, CYPs have significant potential as biocatalysts, and significant efforts are underway to develop them for biocatalytic oxidations either *in vitro* or using whole-cell

Abbreviations: BA, benzoic acid; Bis-Tris, 2,2-Bis(hydroxymethyl)-2,2′,2″-nitrilotriethanol; C(%), coupling efficiency; Cpd 0 (compound 0), the ferric-hydroperoxo intermediate; Cpd I (compound I), the oxy-ferryl porphyrin radical cation species; CYP or P450, cytochrome P450 enzyme; DMSO, dimethylsulfoxide; EPR, electron paramagnetic resonance; EtOH, Ethanol; HaPuR, a flavin-dependent ferredoxin reductase; HaPux, a [2Fe–2S] ferredoxin; H_2O_2, hydrogen peroxide; HPLC, high-performance liquid chromatography; HS, high-spin; K_d, dissociation constant; LS, low-spin; *m*CPBA, *meta*-chloroperoxybenzoic acid; MeCN, acetonitrile; MS, mass spectrometry; NAD(*P*)H, reduced nicotinamide adenine dinucleotide (phosphate); PDB, Protein Data Bank (http://www.rcsb.org/); PEG, polyethylene glycol; PFR, product formation rate; PhIO, iodosylbenzene; *t*BuOOH, *tert*-butyl hydroperoxide; TFA, trifluoroacetic acid; Tris, tris(hydroxymethyl)aminomethane, WT, wild-type..

* Corresponding author.
E-mail address: stephen.bell@adelaide.edu.au (S.G. Bell).

https://doi.org/10.1016/j.jinorgbio.2023.112391
Received 20 August 2023; Received in revised form 30 September 2023; Accepted 2 October 2023
Available online 4 October 2023

systems. [13–15]

The catalytic cycle of these enzymes has multiple steps including separate substrate and dioxygen binding steps, two individual single electron transfers and two proton delivery events. [16,17] The requirement for two electron transfers, at distinct moments in the catalytic cycle, necessitates the use of additional electron transfer proteins to control their delivery from the two electron donating nicotinamide cofactors (NAD(*P*)H). In certain instances, the electron transfer cofactor domains (generally Fe–S clusters or flavins) can be fused to the CYP heme domain, such as in the CYP102A and CYP116B subfamilies of CYP enzymes. [18,19]

In most CYPs, the delivery of the protons is controlled by an acid-alcohol pair of residues located in the I-helix of the enzyme. [20–25] The alcohol residue (threonine or serine) is believed to stabilise the ferric-hydroperoxo intermediate, Compound 0 (Cpd 0), and to alter the pK_a of the distal oxygen to support protonation at this site. [20,26] The role of the acidic residue is hypothesised to be in the shuttling of protons from the surface of the enzyme into the active site to facilitate the two protonation steps. [26] Mutation of the acid residue (aspartate or glutamate) to an amide reduces the rate of the catalytic cycle significantly. [27]

The requirement for electrons, and therefore the ancillary partner proteins, and the nicotinamide cofactors can be eliminated by using peroxides to generate Cpd 0, via a shunt pathway, [28] therefore bypassing several steps of the catalytic cycle. [29,30] Subsequent protonation of Cpd 0 at the distal oxygen induces heterolytic cleavage of the O–O bond to yield the reactive oxy-ferryl porphyrin radical cation species Compound I (Cpd I) with release of a water molecule. [31] Cpd I abstracts a hydrogen from the substrate via the radical rebound mechanism to yield the hydroxylated product. [32,33] Other oxidants such as *tert*-butyl hydroperoxide (*t*BuOOH), [34] *meta*-chloroperbenzoic acid (*m*CPBA) and iodosylbenzene (PhIO) can also be used to drive catalysis with some of these generating Cpd I directly. [28,35]

However, with most CYPs, the pathways using such peroxides or other reactive oxygen donors are inefficient. These reactive oxygen species can cause degradation of the heme (heme bleaching) or react with other residues of the protein resulting in enzyme inactivation. [36] A small subset of CYPs, including the fatty acid oxidising $P450_{BS\beta}$ (CYP152A1), $P450_{SP\alpha}$ (CYP152B1), $P450_{CLA}$ (CYP152A2) and P450 $OleT_{JE}$ (CYP152L1), have evolved to function as peroxygenases using H_2O_2 to drive enzyme activity. [37] These enzymes use the carboxylate group of the fatty acid substrate to reorganise the protons on the hydroperoxy or hydrogen peroxide intermediates to generate Cpd I. Recently, the CYP255 family of cytochrome P450 enzymes, in which the acid-alcohol pair of residues are replaced with an amide and an acid residue, respectively, were demonstrated to function as efficient peroxygenases in addition to having monooxygenase activity and redox partners. [38,39] Other heme peroxygenase enzymes, contain an acid-base residue (histidine, aspartate or glutamate) above the heme for this function. [40–43] Attempts to engineer CYP enzymes for peroxygenase activity have been met with limited success. [44–47] The variants generated so far are often susceptible to destruction by H_2O_2. [36] Recently, mutation of the conserved threonine, of the acid alcohol pair of several CYPs, to a glutamate has been demonstrated to facilitate peroxygenase activity. [45,48] Peroxygenase activity was then engineered into the CYP enzyme CYP199A4 from the bacterium *Rhodospeudomonas palustris* HaA2. [49–51] The T252E variant of CYP199A4 displayed catalytic peroxygenase activity for the oxidative demethylation of 4-methoxybenzoic acid and veratric acid. [49,52–54]

When a suitable hydrophobic substrate binds to a CYP enzyme it displaces the distal water ligand which results in a shift from the low-spin (LS) to the high-spin (HS) ferric form. This can be monitored by UV–visible (UV–Vis) spectroscopy predominantly by the blue shift in Soret band and other spectral changes in the α/β-band region (a Type I shift). [55,56] For example, addition of 4-methoxybenzoic acid to CYP199A4 induces a > 95% spin-state shift from the low-spin (LS) to the high-spin (HS) form indicating that it displaces the distal aqua ligand. However, addition of this substrate to the T252E peroxygenase mutant results in only a ~ 5% shift to the HS state. While the wild-type (WT) enzyme converts 4-methoxybenzoic acid to 4-hydroxybenzoic acid using the monooxygenase pathway at a rate in excess of 1000 min^{-1} the T252E variant demonstrate negligible monooxygenase activity. [53] The structures of CYP199A4 WT enzyme and the T252E variant in complex with 4-methoxybenzoic have been solved by X-ray crystallography to elucidate the binding mode of substrates, and rationalise the spectroscopic changes and the altered activity as described above. [49,50,52] It was observed that in the T252E variant the 6th heme aqua ligand was not displaced by the addition of substrate. This results in this P450 peroxygenase mutant being difficult to reduce and this inhibits dioxygen bonding and subsequent monooxygenase activity. [17,57,58] Based on the X-ray crystal structure and electron paramagnetic resonance (EPR) one of the reasons why this water molecule remains bound is an interaction with the carboxylate group of the introduced glutamate residue. [59]

In this paper we test how tightly the aqua ligand of the T252E variant of CYP199A4 is bound to the ferric heme by investigating the binding of a range of different benzoic acid derivatives. We investigate substrates with larger and more hydrophobic substituents than 4-methoxybenzoic acid. We also tested benzoic acid derivatives which have been shown to directly coordinate to the heme through a nitrogen donor ligand. The interactions of these ligands with the enzyme were tested using a combination of methods including UV–Vis absorbance and EPR spectroscopies, mass spectrometry and X-ray crystallography.

2. Experimental methods

2.1. General

4-Methoxybenzoic acid and 4-*t*-butylbenzoic acid were from Tokyo Chemical Industry (TCI), and 4-benzylbenzoic acid, 4-thiophen-3-ylbenzoic acid, 4-pyridin-2-ylbenzoic acid, pyridin-3-ylbenzoic acid, 4-(1-hydroxyethyl)benzoic acid and 4-(2-hydroxyethyl)benzoic acid were from Fluorochem Ltd. 4-Cyclohexylbenzoic acid, 4-benzoylbenzoic acid and 4-phenylbenzoic acid were from Alfa Aesar, and 4-(1*H*-imidazol-1-yl)benzoic acid was from Maybridge (Thermo Fisher Scientific). 4-Ethylbenzoic acid, 4-vinylbenzoic acid, 4-methylthiobenzoic acid and 4-isopropylbenzoic acid were from Sigma-Aldrich. Sodium dithionite, ethanol, DMSO and hydrogen peroxide (30% *w*/w) were from Chem-Supply. Bovine liver catalase was from Sigma-Aldrich, and NADH disodium salt trihydrate was purchased from VWR International, LLC. Tris (ultrapure grade), dithiothreitol (DTT), and isopropyl β-D-1-thiogalactopyranoside (IPTG) were from Astral Scientific. Trifluoroacetic acid (TFA) was from Sigma-Aldrich and acetonitrile (HPLC grade) was from Ajax Finechem. Paratone-N oil (Parabar 10,312) and PEG (polyethylene glycol) 3350 were from Hampton Research, and MicroMounts, MicroLoops and MicroTools were purchased from MiTeGen, LCC. High vacuum grease was from Dow Corning.

A Cary 60 UV–Vis spectrophotometer (Agilent Technologies) coupled to a Peltier unit was used to record UV–Vis spectra and kinetic traces at 30 ± 0.5 °C; a quartz cuvette was used with a path length of 10 mm. Analytical high-performance liquid chromatography (HPLC) was performed using a Kinetex XB-C18 reversed-phase liquid chromatography column (100 Å pore size, 250 × 4.6 mm, 5 μm; Phenomenex). A gradient of 20–95% acetonitrile in water (with 0.1% TFA) was used to elute the samples at a rate of 1 mL min^{-1} and the eluate was monitored at 254 nm. The instrument used was an Agilent 1260 Infinity system.

2.2. Production and purification of CYP199A4

The T252E mutant of CYP199A4 was produced and purified according to the published procedure. [60,61] The purified P450 enzyme was filter-sterilized using a Minisart Syringe Filter (pore size: 0.2 μm)

and stored in ~50% glycerol at −20 °C. Before use, aliquots of the T252E CYP199A4 stock solution were desalted by gel filtration chromatography, using a PD-10 desalting column (Cytiva) and Tris-HCl buffer (50 mM, pH 7.4) as the eluent. The P450 was quantified using an extinction coefficient of $\varepsilon_{419} = 119\ mM^{-1}\ cm^{-1}$. [60]

2.3. Substrate binding and dissociation constant analysis

The UV–Vis absorbance spectral shifts induced by binding potential substrates to T252E CYP199A4 were measured as described previously. [61] A baseline spectrum was first recorded with Tris-HCl buffer (50 mM, pH 7.4) and the UV–Vis absorption spectrum of 500 or 600 μL of a desalted T252E CYP1994 solution (~1 μM) was recorded from 700 to 250 nm. Other experiments were also done in 50 mM Tris-HCl, 8.0 or 9.0 or 50 mM Bis-Tris buffer, pH 5.5. The UV–Vis scan rate was 600 nm/min and the data interval was 1 nm. Substrate (1–10 μL aliquots) was added from a 25-, 50- or 100-mM substrate stock solution (recording the UV–Vis spectrum after each addition) until no further spectral change occurred. For methyl *p*-anisate, a 25 mM stock solution was prepared in ethanol. For 4-pyridin-3-ylbenzoic acid, a 50 mM stock solution was prepared in DMSO, whereas a 100 mM stock solution of 4-pyridin-2-ylbenzoic acid was prepared in DMSO. For 4-(1*H*-imidazol-1-yl)benzoic acid, a 25 mM stock solution was prepared in Tris buffer (50 mM, pH 9.5). For the other substrates, a 100 mM stock solution was prepared in EtOH/DMSO. The change in the UV–Vis absorbance spectrum of WTCYP199A4 induced by sterically bulky substrates were measured for comparison.

UV–Vis titrations were performed according to the published method to determine the substrate binding affinity (K_d values). [60] Each titration was performed in triplicate using a Cary 60 UV–Vis spectrophotometer. The UV–Vis scan rate was 600 nm/min and the data interval was 1 nm. K_d values were determined for 4-methoxybenzoic acid, 4-vinylbenzoic acid, 4-methylthiobenzoic acid, 4-ethylbenzoic acid, 4-cyclohexylbenzoic acid, 4-*t*-butylbenzoic acid, 4-pyridin-2-ylbenzoic acid and 4-pyridin-3-ylbenzoic acid with T252E CYP199A4. First, a baseline spectrum was recorded using 2.5 mL of a solution of T252E CYP199A4 in Tris-HCl buffer (50 mM, pH 7.4) (P450 concentration: 1.5–2.8 μM). Aliquots (0.5–5 μL) of a 1-, 10- or 100-mM substrate stock solution (in EtOH/DMSO) were successively added using a Hamilton syringe. A maximum of >10 μL of each stock solution was added to avoid significantly diluting the enzyme. (Note that for the 4-pyridin-2-ylbenzoic acid titration, 0.1, 1 and 10 mM stock solutions in DMSO were used). The UV–Vis difference spectrum was recorded after each addition of substrate from 600 to 300 nm. The peak-to-trough absorbance difference ($\Delta A = A_{peak} - A_{trough}$) was then plotted against the substrate concentration [*S*]. All substrates displayed tight binding ($K_d \leq 5 \times$ [P450]) and the data were therefore fitted to the Morrison tight-binding equation:

$$\Delta A = \Delta A_{max} \times \frac{[E] + [S] + K_d - \sqrt{([E] + [S] + K_d)^2 - 4[E][S]}}{2[E]}$$

where [*E*] is the P450 concentration, K_d is the dissociation constant, [*S*] is the substrate concentration, ΔA is the peak-to-trough absorbance difference and ΔA_{max} is the maximum peak-to-trough absorbance difference.

2.4. X-ray crystallography

X-ray crystal structures of T252E CYP199A4 bound to the sterically bulky substrates were obtained by following the published method. [60,61] A desalted solution of T252E CYP199A4 in Tris-HCl buffer (50 mM, pH 7.4) was first concentrated to 35–40 mg/mL using a Microsep Advance centrifugal device with a 10 kDa MWCO membrane (Pall Corporation). The concentrated protein was complexed with 2–4 mM substrate (added from a 100 mM stock solution in EtOH/DMSO). Each P450-ligand complex was crystallised via the hanging-drop vapour-diffusion method, using 24-well trays and the previously reported crystallisation conditions. Hanging drops consisted of 1 μL of the protein-ligand complex mixed with 1 μL of the reservoir solution. Each drop was equilibrated against a 500 μL aliquot of reservoir solution at 16 °C. The reservoir solution contained: 100 mM Bis-Tris buffer (pH 5.00, 5.25, 5.50 or 5.75), 0.2 M magnesium acetate, and 20, 23, 26, 29, 30.5 or 32% PEG (polyethylene glycol) 3350. Crystals were harvested using MicroMounts or MicroLoops, coated in Paratone-N oil as the cryoprotectant and flash frozen in liquid nitrogen. Diffraction data for the crystal of 4-(pyridin-2-yl)benzoic acid-bound T252E CYP199A4 was collected on the MX1 beamline at the Australian Synchrotron. [62] The data for the crystals of T252E CYP199A4 bound to 4-thiophen-3-ylbenzoic acid and 4-benzylbenzoic acid was collected on the MX2 beamline. [63] The exposure time was 1 s, oscillation angle 1° and wavelength 0.9537. For the 4-pyridin-2-ylbenzoic acid structure, iMosflm [64] was used to index and integrate the data, and the data were then scaled and merged using Aimless (part of the CCP4 suite of programs). [65] For the 4-thiophen-3-ylbenzoic acid and 4-benzylbenzoic acid structures, the data were automatically processed at the Australian Synchrotron using *xdsme* and Aimless. [66,67] PhaserMR in the CCP4 suite of programs was used to solve the structure by the molecular replacement method. [68] A high-resolution (1.54-Å resolution) structure of CYP199A4 (PDB code: 5UVB, with the heme, chloride, 4-cyclopropylbenzoic acid substrate and waters deleted) was used as the search model. Positive density in the difference map revealed the position of the Glu252 side chain and the ligand in the active site. Coordinates and restraints for the ligand were generated using Phenix eLBOW [69] and the protein model was manually rebuilt in Coot. [70] Refinement was performed using phenix.refine and this was followed by multiple rounds of manual rebuilding in Coot and refinement to improve the model. [71] Solvent was added automatically using phenix.refine and positive density in the anion binding site of CYP199A4 was modelled as a chloride ion. [49] The validation tool *MolProbity* [72] was used to assess the quality of the model before the structure was deposited into the Protein Data Bank (www.rcsb.org). Composite omit maps and feature-enhanced maps were generated using Phenix. [73–75] Images of the refined crystal structures were generated using PyMOL. [76]

2.5. NADH activity assays

In vitro NADH activity assays for WT and T252E CYP199A4 with 4-ethylbenzoic acid were performed according to the previously described method. [60] Reactions were performed at 30 °C on a 600 μL- or 1200 μL-scale in a quartz cuvette and contained 0.5 μM CYP199A4 (WT or T252E mutant), 5 μM HaPux, 0.25 μM HaPuR and 100 ng μL^{-1} bovine liver catalase in freshly oxygenated Tris-HCl buffer (50 mM, pH 7.4). This solution was used to set the absorbance reading of the UV–Vis spectrophotometer at 340 nm to zero. The mixture was incubated at 30 °C for 2 min before NADH was added to a concentration of ~320 μM, corresponding to an absorbance of ~2.0. The rate of NADH background oxidation (the 'leak' rate) was measured before initiating the reaction. To start the reaction, 1 mM substrate was added from a 100 mM stock in EtOH/DMSO and NADH depletion was monitored at 340 nm. The rate of NADH consumption (*N*) by the P450 enzyme in units of (μM-NADH) $(\mu M\text{-P450})^{-1}\ min^{-1}$ was calculated from the slope of the graph of Abs340 versus time using an extinction coefficient of $\varepsilon_{340} = 6.22\ mM^{-1}\ cm^{-1}$. The units are abbreviated to min^{-1}.

$$N = \frac{\frac{\Delta Abs_{340}}{\Delta time} \times 1000 \times 2}{6.22}$$

A modified method was used for the T252E mutant. The rate of NADH consumption by the T252E mutant was exceedingly slow and therefore half the amount of NADH (~160 μM rather than 320 μM) was added to each reaction. After substrate was added, NADH consumption was monitored by UV–Vis spectroscopy at 30 °C for the first ~15 min.

The reaction mixture was then left at room temperature until all NADH had been consumed. NADH consumption rates reported for the T252E mutant are the initial rates over the first 10 min. Control reactions were also performed in which either the P450 or NADH was omitted from the turnover mixture (replaced with the same volume of buffer).

Products were identified and quantitated by HPLC. To prepare turnover mixtures for HPLC analysis, 132 μL of the *in vitro* turnover mixture was mixed with 66 μL of MeCN (acetonitrile) and 2 μL of internal standard (10 mM 9-hydroxyfluorene in EtOH) and centrifuged to remove particulate matter. Products were identified by co-elution with pure authentic samples of the expected oxidation products. Calibration curves were constructed to quantify the product. If authentic samples of the oxidation products were unavailable, calibration curves were constructed using structurally similar compounds to estimate the amount of product. Pure authentic 4-oxiran-2-ylbenzoic acid was unavailable so this product was quantified using 4-(1-hydroxyethyl)benzoic acid.

2.6. H_2O_2-driven reactions

4-Hour reactions were performed at 30 °C in duplicate on a 600-μL scale and contained 1 mM 4-benzylbenzoic acid (added from the 100 mM stock solution in EtOH/DMSO), 3 μM of CYP199A4 and 50 mM H_2O_2 (added from a freshly prepared 200 mM H_2O_2 stock solution) in Tris-HCl buffer (50 mM, pH 7.4). The H_2O_2 was added last to initiate each reaction. Control reactions were also performed that omitted the P450 (which was replaced with an equal volume of Tris buffer) or contained 3 μM CYP101B1 instead. (An extinction coefficient of ε_{417} = 113 mM^{-1} cm^{-1} was used to quantify the CYP101B1 protein.) A control reaction was also performed using 3 μM denatured T252E CYP199A4, which was first heated at 80 °C for 45 min to denature it. After 4 h, a 132 μL aliquot of each reaction mixture was quenched by mixing it with 10 μL of bovine liver catalase solution (10 mg/mL) and 66 μL of acetonitrile. The samples were centrifuged to eliminate precipitate/particulate matter and were analysed by HPLC using a gradient of 20–95% acetonitrile (MeCN) in H_2O (with 0.1% TFA).

2.7. UV–Vis absorbance spectra of ferrous T252E CYP199A4 in complex with substrates and type II inhibitors

The UV–Vis absorbance spectrum of 1 mL of a solution of T252E CYP199A4 was recorded as described above and the protein was then saturated with substrate/inhibitor (≥1 mM). Sodium dithionite was added to reduce the heme and the spectrum of the ferrous P450 complex was recorded.

In case the T252E mutant was not being reduced by this method, we attempted to reduce the T252E mutant more fully by incubating it with dithionite on ice before addition of substrate. The UV–Vis spectrum of 500 μL of substrate-free T252E CYP199A4 in 50 mM Tris-HCl buffer (pH 7.4) was recorded and a half spatula-tipful of dithionite was then added to reduce the P450. The solution was incubated on ice for 10–30 min. The reduced P450 was subsequently saturated with ligand (≥1 mM) and the spectrum of the ferrous T252E CYP199A4-ligand complex was recorded. After addition of 4-pyridin-3-ylbenzoic acid, the mixture was incubated on ice for a further 30 min before the spectrum was recorded.

2.8. Native MS

All native mass spectrometry experiments were performed on a linear trap quadrupole-orbitrap MS (LTQ Orbitrap XL; Thermo Fisher Scientific, MA, USA) that was equipped with a nanoelectrospray ionization source. Nanoscale ion emitters were prepared from borosilicate glass capillaries (Harvard Apparatus, 1.2 mm o.d., 0.68 mm i.d.) with inner tip diameters of 250 nm using a microcapillary puller (Model P-97, Sutter Instruments, Novato, CA, USA). The borosilicate ion emitters were coated with a thin layer of gold and palladium at a molar ratio of 1:1 using a metal sputter coater (Scancoat Six, Edwards, UK). For nESI-MS experiments, each capillary emitter was loaded with ~3 μL of the sample solution using an autopipette (10 μL capacity, Eppendorf, Germany) and tip (20 μL capacity GELoader, Eppendorf, Germany). nESI emitters were positioned ~2 mm on axis from the heated capillary entrance (250 °C) to the MS. A voltage of +0.8 to +1.5 kV was applied to the nESI emitters relative to the capillary entrance of the mass spectrometer and a maximum ion accumulation time of 500 ms was used throughout. For native mass spectra, triplicate measurements were acquired for 2–3 min using three different ion emitter tips. For each mass spectrum, peak areas corresponding to the unbound and ligand-bound proteins were integrated using MATLAB (version 2017a, MathWorks, USA). The dissociation constants from native MS data for ligand binding to the CYP199A4 and T252E mutant were obtained using an analytical derived equation: [77].

$$K_{d,i} = \frac{\sum_n P^{n+}}{\sum_n PL_i^{n+}} \left([L_i]_0 - \frac{\sum_n PL_i^{n+}}{\sum_n P^{n+} + \sum_i \sum_n PL_i^{n+}} [P]_0 \right) \quad (1)$$

in which $K_{d,i}$ corresponds to the dissociation constant of the *i*th ligand (L_i); P^{n+} and PL_i^{n+} correspond respectively to the ion abundances of the unbound protein and L_i-bound complex; and $[L_i]_0$ and $[P]_0$ correspond to the initial concentrations of the ligands and protein, respectively.

2.9. EPR spectroscopy

X-band ($\nu_{average}$ = 9.75162 GHz) CW EPR was performed at 15 K using a Bruker E500 spectrometer in a Bruker spherical SHQ cavity and liquid helium cryostat (from Oxford Instruments). CW EPR data was measured with a modulation amplitude of 0.5 mT, a 100 kHz modulation frequency, and under non-saturating conditions. Calibration of the magnetic field was performed with a 2,2-diphenyl-1-picrylhydrazyl (DPPH) standard, g = 2.0036.

Pulse X-band ($\nu_{average}$ = 9.73907 GHz) EPR spectra were measured at 12.5 K using a Bruker E580 spectrometer in a 4 mm Bruker split-ring dielectric pulse resonator with a 1 kW TWT microwave amplifier as described previously. [78] EPR data were processed using MATLAB 9.10.0.1602886 (R2021a) (The MathWorks, Inc.).

3. Results and discussion

3.1. Binding of para-substituted benzoic acid substrates to T252E CYP199A4

The changes in the UV–Vis absorbance spectrum induced by binding various other *para*-substituted benzoic acids to T252E CYP199A4 were measured to determine whether these substrate can displace the 6th water/hydroxide (H_2O/OH^-) ligand (Table 1, Fig. 1 and Fig. S1). 4-Vinyl-, 4-methylthio-, 4-ethyl-, and 4-isopropyl-benzoic acid are reported to all induce large (≥70% - 95%) type I shifts when they bind to WT CYP199A4 (Table 1). [50,53]

Table 1
The changes in the UV–Vis absorbance spectrum induced by binding of various substrates to the T252E mutant of CYP199A4. Shifts for the WT enzyme, previously reported by others, are included for comparison. [52,53,80] Several substrates induced small red-shifts in the Soret band maximum (λ_{max}) of T252E CYP199A4; these red-shifts are shown in Fig. S1.

Substrate	UV–Vis Spectral Changes (% HS)	
	T252E	WT
4-methoxyBA	5%	≥95% [53]
4-ethylBA	<5%	≥95% [52]
4-vinylBA	~0.5 nm red-shift	80%
4-methylthioBA	~1.5 nm red-shift	70% [52]
4-methoxybenzamide	5%	≥95% [80]
methyl *p*-anisate	<5%	<5% [80]

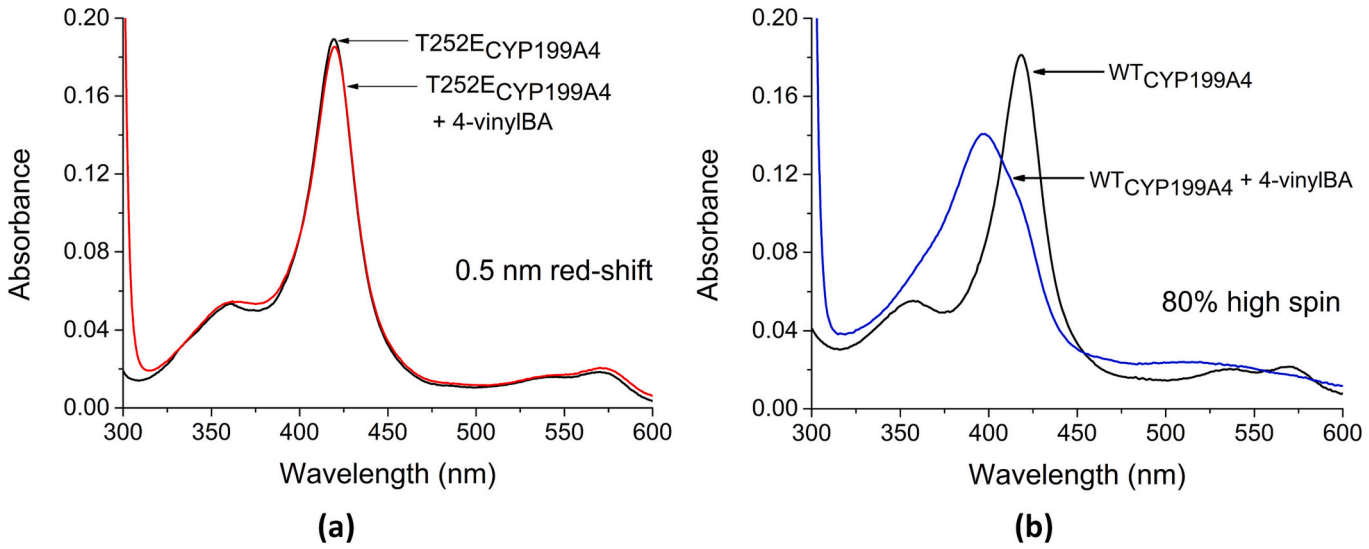

Fig. 1. (a) The change in the UV–Vis absorbance spectrum of the T252E mutant of CYP199A4 induced by 4-vinylbenzoic acid (~0.5 nm red-shift), **(b)** and the change associated with the spin-state shift of WT CYP199A4 induced by 4-vinylbenzoic acid (80% high spin). (For interpretation of the references to colour in this figure legend, the reader is referred to the web version of this article.)

4-Ethylbenzoic acid, which has a more hydrophobic substituent and may be more likely to displace the ferric heme-bound aqua ligand, induced only a minor type I shift (<5%) (Fig. S1). No changes occurred in the α/β band region. Addition of several of these substrates resulted in a small red-shift of the Soret band. A spectrum with a red shifted Soret can result when a stronger field ligand than water coordinates to the ferric iron of the heme. [79] The sulfur-containing ligand 4-methylthiobenzoic acid red-shifted the Soret band by ~1.5 nm (Fig. S1). 4-Vinylbenzoic acid induced a smaller (~0.5 nm) red-shift (Figs. S1a).

In case the mutation had substantially altered the active-site structure and the enzyme was now unable to bind benzoic acid derivatives, we tested substrates with alternative functional groups *para* to the methoxy group (4-methoxybenzamide and methyl *p*-anisate). None of these substrates induced any appreciable change that would be associated with change in the spin-state of ferric heme (Table 1, Fig. S1c).

Due to the minimal changes in the UV–Vis absorption spectrum induced by substrate binding to the T252E mutant, only approximate values for the substrate binding affinity (K_d) could be obtained by performing UV–Vis titrations (Fig. S2, Table 2). As the lack of any significant spectral changes prevented accurate measurement of binding affinity, a native mass spectrometry method was also used to measure the binding affinity (Table 2 and see Supporting Information for further details). [77,81,82] These demonstrate that the T252E mutant retains the ability to bind *para*-substituted benzoic acid substrates tightly. Evidently, the Thr → Glu mutation has not impaired the enzyme's ability to bind *para*-substituted benzoic acids.

Table 2
Binding affinity of the T252E variant of CYP199A4 for *para*-substituted benzoic acid substrates. K_d values were determined by performing UV–Vis titrations and were analysed using a native mass spectrometry method. [77] Literature K_d values for WT CYP199A4 are provided for comparison.

	T252E		WT
Substrate	K_d (μM) UV–Vis titration[a]	K_d (μM) Mass spectrometry	K_d (μM) UV–Vis titration
4-methoxyBA	0.4 ± 0.1	1.11 ± 0.04	0.22 ± 0.02 [52]
4-vinylBA	0.1 ± 0.1	0.58 ± 0.02	0.46 ± 0.03
4-methylthioBA	0.1 ± 0.1	0.84 ± 0.08	2.3 ± 0.3 [52]
4-ethylBA	0.7 ± 0.2	2.3 ± 0.2	0.34 ± 0.02 [52]

[a] UV–Vis titrations were performed in triplicate.

Previously we have demonstrated that the T252E variant does not efficiently utilise NADH/O_2 when coupled to the physiological electron transfer partners to oxidise 4-methoxybenzoic acid (Table S1). We confirmed that this was the case by using the T252E variant to catalyse the oxidation of 4-ethylbenzoic acid (Table S1). The rate of NADH consumption by the T252E mutant was exceedingly slow, the coupling efficiency was reduced and low levels of the oxidised metabolites were produced in line with the previous observations that this mutation has largely abolished the enzyme's ability to utilise NADH/O_2 to perform monooxygenation reactions (Table S1). The product distribution of 4-ethylbenzoic acid oxidation by the T252E enzyme was comparable to that of the WT enzyme resulting in metabolites which arise from hydroxylation and desaturation (Table S2 and Fig. S3 and S4). This confirms that these substrates do bind to within the active site in a similar manner to the WT enzyme. However, the spectroscopic data above infers that the 6th aqua ligand is not displaced and this is in agreement with the low monooxygenase activity observed which would arise due to inhibition of the 1st electron transfer step and/or dioxygen binding.

3.2. Binding of bulky hydrophobic ligands and type II binding ligands to the T252E mutant

To further probe how tightly the distal 6th ligand is bound to the iron, we attempted to displace it using various bulky hydrophobic substrates (4-thiophen-3-ylbenzoic acid, 4-benzylbenzoic acid, 4-cyclohexylbenzoic acid, 4-phenylbenzoic acid, 4-isopropylbenzoic acid and 4-*t*-butylbenzoic acid). We reasoned that these substrates, due to their steric bulk, would have greater likelihood of displacing the ligand. When added to WT CYP199A4, they all induce large shifts to the high-spin form (≥90% HS). [50] However, when added to the T252E mutant none of these substrates induced a substantial shift in the UV–Vis absorption spectrum indicating that the aqua ligand had not been displaced (Table 3 and Fig. S5). The sulfur-containing ligand 4-thiophen-3-ylbenzoic acid induced a ~ 1.0 nm red-shift in the Soret band position, whereas 4-phenyl- and 4-benzyl-benzoic acid induced ~0.5 nm red-shifts (Fig. S6). 4-Cyclohexylbenzoic acid and 4-*t*-butylbenzoic acid both induced a ~ 10% shift to HS CYP199A4 (Fig. S5, Table 3). The binding affinity of T252E with 4-cyclohexylbenzoic acid and 4-*t*-butylbenzoic acid were determined. That of 4-cyclohexylbenzoic acid was found to be comparable to that with the WT enzyme while *t*-butylbenzoic acid bound more tightly to the mutant (Table S3 and Figs. S7 and

Table 3
The change in the UV–Vis absorption spectrum induced by binding of various bulky substrates to the T252E mutant of CYP199A4. Shifts for the WT enzyme, previously reported by others, are included for comparison. 4-Benzyl-, 4-thiophen-3-yl- and 4-phenyl-benzoic acid induced small red-shifts in the Soret band from 419.5 → 420.0 or 420.5 nm upon binding to T252E CYP199A4 (Fig. S6).

Substrate	UV–Vis Spectral Changes (% HS)	
	T252E	WT
4-benzylBA	~0.5 nm red-shift	90% [83]
4-thiophen-3-ylBA	~1.0 nm red-shift	90% [84]
4-cyclohexylBA	~10%	≥95% [85]
4-phenylBA	~0.5 nm red-shift	90% [85]
4-isopropylBA	~10%	≥95% [50]
4-*t*-butylBA	~10%	90% [50]
4-pyridin-2-ylBA	~3 nm red-shift	3 nm red-shift [78]
4-pyridin-3-ylBA	~3.5 nm red-shift	5 nm red-shift [78]

S8).

To confirm binding and activity of the substrates within the active site we investigated whether the T252E mutant could oxidise 4-benzylbenzoic acid, using H_2O_2. We found that the T252E mutant could indeed utilise H_2O_2 to convert 4-benzylbenzoic acid with the same regioselectivity as the WT enzyme (Fig. 2). However, there was a switch in the enantioselectivity of the 4-(hydroxy(phenyl)methyl)benzoic acid metabolite generated using the T252E peroxygenase versus the WT monooxygenase reaction (Fig. S9).

As we were unable to displace the ferric heme-bound ligand using various sterically bulky substrates, we next used nitrogen donor ligands in an attempt to displace the water. We previously demonstrated that 4-pyridin-3-ylbenzoic acid directly coordinates to the iron in WT CYP199A4, but 4-pyridin-2-ylbenzoic acid instead hydrogen-bonds to the heme-bound water. [78] 4-Pyridin-2-ylbenzoic acid and 4-pyridin-3-ylbenzoic acid induce different type II UV-spectral shifts when they bind to WT CYP199A4. [78] These substrates were also found to induce red-shifts of the Soret band when they were added to the T252E mutant (Fig. 3, Table 3 and Table S4). 4-Pyridin-2-ylbenzoic acid induced a ~ 3 nm shift and 4-pyridin-3-ylbenzoic acid a ~ 3.5 nm shift. 4-Pyridin-2-ylbenzoic acid was found to bind more tightly to the T252E mutant than to WT CYP199A4 (0.10 ± 0.01 vs. 1.0 ± 0.1 μM) (Figs. S7, S8 and S10, Table S5). On the other hand, 4-pyridin-3-ylbenzoic acid displayed lower affinity for the T252E mutant than for the WT enzyme (7.9 ± 0.1 vs. 2.3 ± 0.1 μM).

For the T252E mutant, the absolute and difference spectra induced by 4-pyridin-2-ylbenzoic acid and 4-pyridin-3-ylbenzoic acid are almost indistinguishable (Fig. 3). They do not resemble the spectrum of WT CYP199A4 with 4-pyridin-3-ylbenzoic acid bound but instead both take after the spectrum induced by 4-pyridin-2-ylbenzoic acid. The magnitude of the red-shift is almost the same for both ligands (~3 vs. ~3.5 nm), and the α-band remains more intense than the β-band (Fig. 3). This is a characteristic of CYPs in complex with oxygen donor ligands. [86,87] There is also no increase in the intensity of the δ-band. This is evidence that 4-pyridin-3-ylbenzoic acid does not displace the water in the T252E mutant. Similar differences between the WT and T252E mutant were obtained with the type II ligand 4-1*H*-imidazol-1-ylbenzoic acid, suggesting retention of the oxygen donor ligand in the T252E variant (Fig. S10). There were some differences in the UV–Vis absorbance spectral changes between the imidazolyl and pyridinyl ligands with both the WT and T252E mutant of CYP199A4 (Fig. S10).

Ferrous CYP199A4 with directly bound σ-donor nitrogen ligands displays a red-shifted Soret peak at ~442 nm. [78,88] In an attempt to confirm that the nitrogen ligands were not directly bound to the iron in the T252E variant, we added dithionite to reduce the heme in the presence of the pyridinyl compounds. However, as previously reported, the T252E variant, unlike the WT enzyme, was difficult to reduce using this method (Figs. S10 – S13). [59]

3.3. EPR data

EPR experiments were performed to further evaluate the ferric heme coordination environment after the binding of selected substrates to the T252E mutant. There was no evidence of high-spin heme signals in the continuous-wave (CW) EPR spectrum of T252E CYP199A4 (Fig. S14). However, two low-spin components, A1 and A2, were present in all the substrate-bound and substrate-free spectra with the exception of A1 which was absent from the 4-pyridin-2-ylbenzoic acid sample (Fig. 4, and Fig. S14). A2 is absent from the spectra of WT CYP199A4. [78] The A1 component resembled those of a low-spin six-coordinate aqua ligated ferric heme (Fig. 4 and Fig. S15). A2 in the T252E samples had a higher g_z value (2.52–2.55), in line with what was reported previously with the 4-methoxybenzoic acid-T252E complex (Fig. 4 and Fig. S15). [59] For P450s with water bound as the sixth ligand, $g_z \leq 2.45$, and larger g_z values, such as those for component A2, are associated with low-spin ferric P450s with nitrogen or anionic ligands bound. [78]

The EPR for 4-pyridin-2-ylbenzoic acid in complex with the T252E

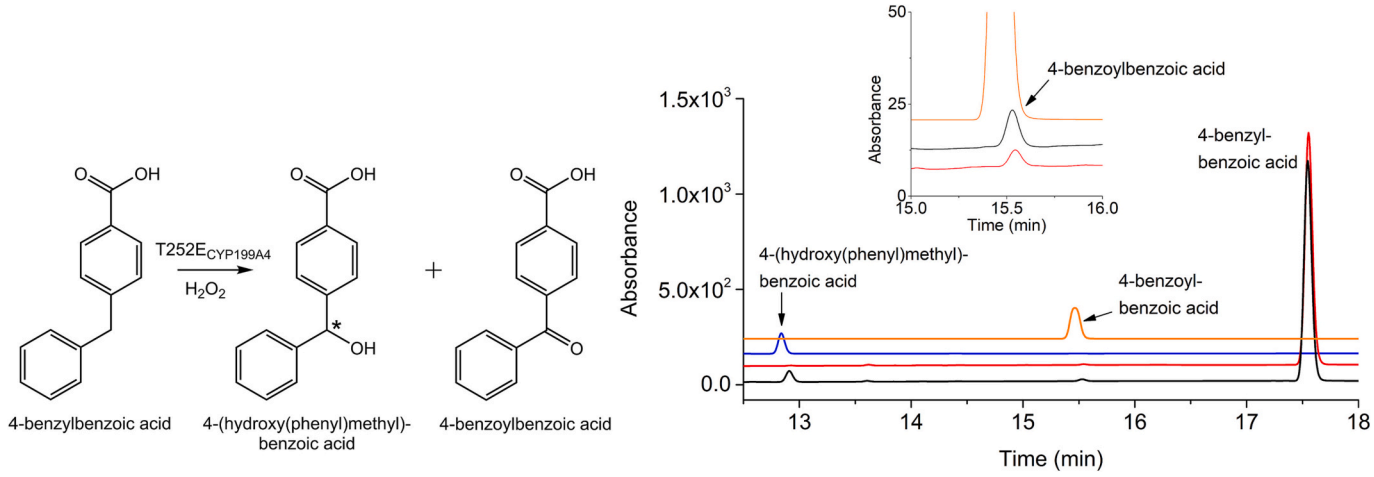

Fig. 2. HPLC analysis of the H_2O_2-driven oxidation of 4-benzylbenzoic acid by T252E CYP199A4. In **black** is the *in vitro* reaction, in red is a control reaction performed with heat-denatured T252E enzyme, in blue is authentic 4-(hydroxy(phenyl)methyl)benzoic acid (RT = 12.8 min) synthesised and purified by HPLC and in orange is authentic 4-benzoylbenzoic acid (RT = 15.5 min). The substrate appears at 17.6 min. Conditions: 3 μM P450, 50 mM H_2O_2, reaction time = 240 min, T = 30 °C. Gradient: 20–95% acetonitrile in H_2O with 0.1% trifluoroacetic acid. Detection wavelength: 254 nm. (For interpretation of the references to colour in this figure legend, the reader is referred to the web version of this article.)

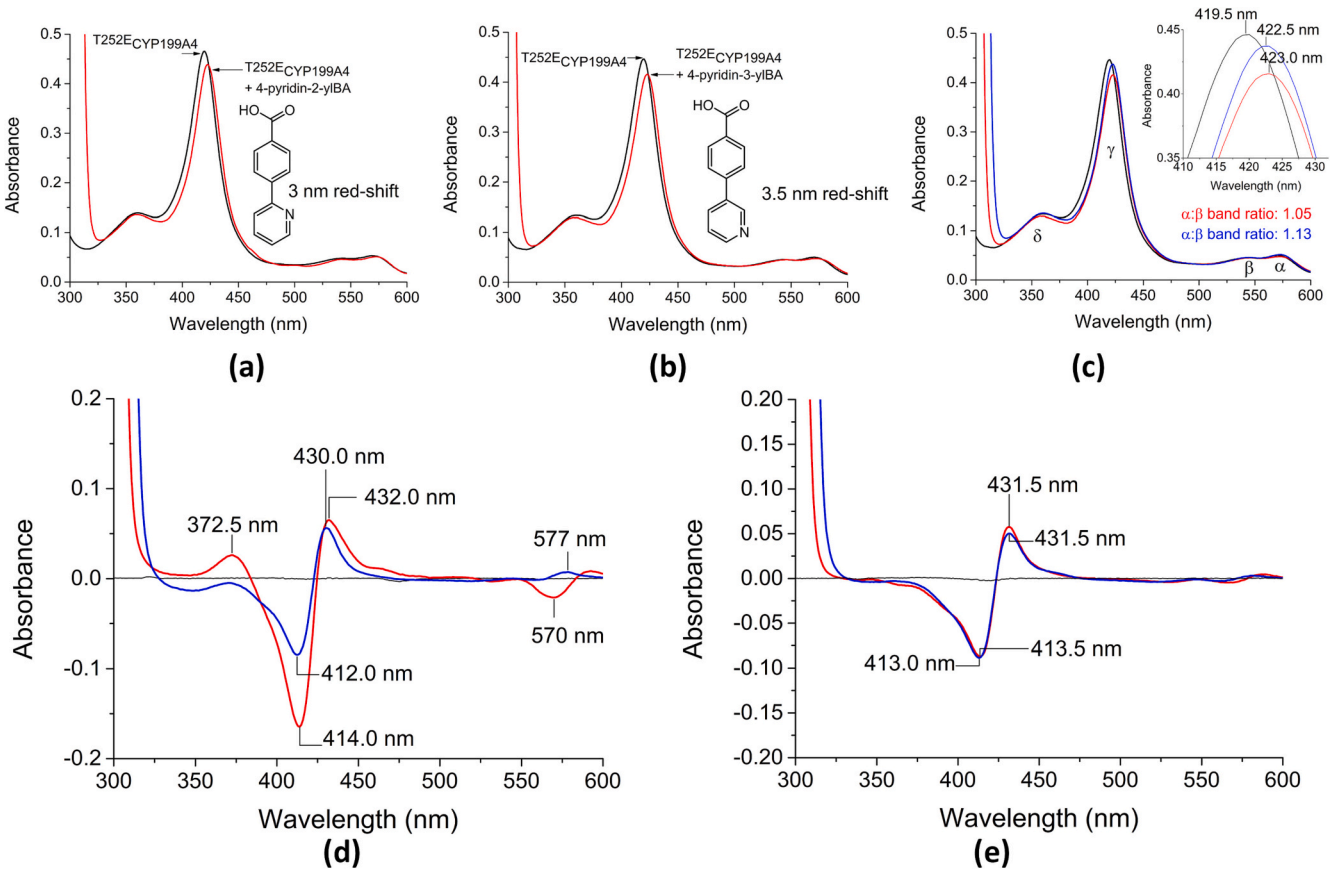

Fig. 3. The change in the UV–Vis absorbance spectrum of the T252E mutant of CYP199A4 induced by **(a)** 4-pyridin-2-ylbenzoic acid, and **(b)** 4-pyridin-3-ylbenzoic acid. (c) An overlay of the UV–Vis spectra of T252E CYP199A4 bound with 4-pyridin-3-ylbenzoic acid (red) and 4-pyridin-2-ylbenzoic acid (blue). In black is substrate-free enzyme. (d) Difference spectra of WT CYP199A4 with 4-pyridin-3-ylbenzoic acid (red) and 4-pyridin-2-ylbenzoic acid (blue). The enzyme concentration was 5.2 μM. (e) Difference spectra of T252E CYP199A4 with 4-pyridin-3-ylbenzoic acid (red) and 4-pyridin-2-ylbenzoic acid (blue). The enzyme concentration was 3.7 μM. (For interpretation of the references to colour in this figure legend, the reader is referred to the web version of this article.)

variant contains a single species with the higher than expected g_z value, A2 (2.52 versus 2.44 for the WT enzyme; Fig. S15 and Table S6). Based on the UV–Vis absorbance spectrum we hypothesize that this signal is due to an aqua bound-ferric heme in which the aqua ligand is interacting with a nitrogen ligand and potentially the E252 residue. For comparison, the WT CYP199A4 4-pyridin-3-ylbenzoic acid complex one component (94%) of the EPR spectrum had a g_z value of 2.52 (Table S6). This was consistent with the direct coordination of nitrogen to the heme observed in the crystal structure for 4-pyridin-3-ylbenzoic acid. [78] In the T252E mutant with this ligand there were two components to the spectrum with g_z values (A1, 2.46 and A2, 2.54). This agrees with the other complexes reported here which do not displace the 6th axial water ligand (Fig. 4 and Fig. S15). The higher g_z value of the A2 components in these systems may arise due to the coordination environment of the aqua ligand resulting in it having stronger ligand field character.

Given the closeness of the g_z values of the direct nitrogen coordinated 4-pyridin-3-ylbenzoic acid-bound WT CYP199A4 and the second component of the ligand-bound forms of the T252E mutant, which we propose is due to an aqua-ligand bound ferric heme but in a different environment, we performed HYSCORE pulse EPR experiments on these samples. [78] The ^{1}H regions of these spectra show significant signals belonging to ^{1}H nuclei close to the ferric center, suggesting water is the 6th axial ligand in both the 4-pyridin-3-yl- and 4-pyridin-2-yl-benzoic acid T252E samples (Fig. S16). [59] Importantly there was no evidence of ^{14}N HYSCORE signals in addition to the normal peaks from the ^{14}N pyrrole nitrogens in either species which would indicate direct nitrogen coordination to the heme and are observed for 4-pyridin-3-yl-benzoic acid with the WT enzyme. [78,89]

At the temperatures used for EPR experiments the pH of the buffer can change. The temperature and pH are known to potentially alter the heme environment of CYP enzymes. [90,91] In an effort to better understand the effects of pH on the electronic structure of the T252E variant we analysed the UV–Vis absorbance spectrum at different pH values (Fig. S17). At higher pH 8.0 and 9.0 the UV–Vis absorbance spectrum of T252E bound to 4-methoxybenzoic acid was similar to that obtained at pH 7.4 (Fig. S17). At pH 5.5 there was a prominent shoulder at 390 nm indicating a mixture of species. Altering the temperature did not change the UV–Vis absorbance spectrum (Fig. S17).

3.4. Crystal structures

We were able to obtain crystals of the T252E mutant of CYP199A4 soaked with several of the bulky substrates tested above. The crystals of 4-*t*-butylbenzoate-bound T252E CYP199A4 diffracted poorly and were not pursued further. The crystal structure of T252E CYP199A4 in complex with 4-isopropylbenzoic acid was solved. However, while the electron density of the benzoic acid moiety could be distinguished that of the isopropyl methyl groups was not visible (Fig. S18). Crystal structures of the T252E mutant in complex with 4-benzylbenzoic acid and 4-thiophen-3-ylbenzoic acid were determined. The electron density for the ligand was observed and these confirmed that the bulky ligands had not displaced the water (Figs. 5 and 6).

The crystal structures of 4-benzyl- and 4-thiophen-3-yl-benzoate-bound T252E CYP199A4 were solved at resolutions of 1.79 and 2.02 Å, respectively (Table S7 and Figs. S19 and S20). The refined occupancy of the H_2O/OH^- ligand was 95% in the 4-benzylbenzoate-bound T252E

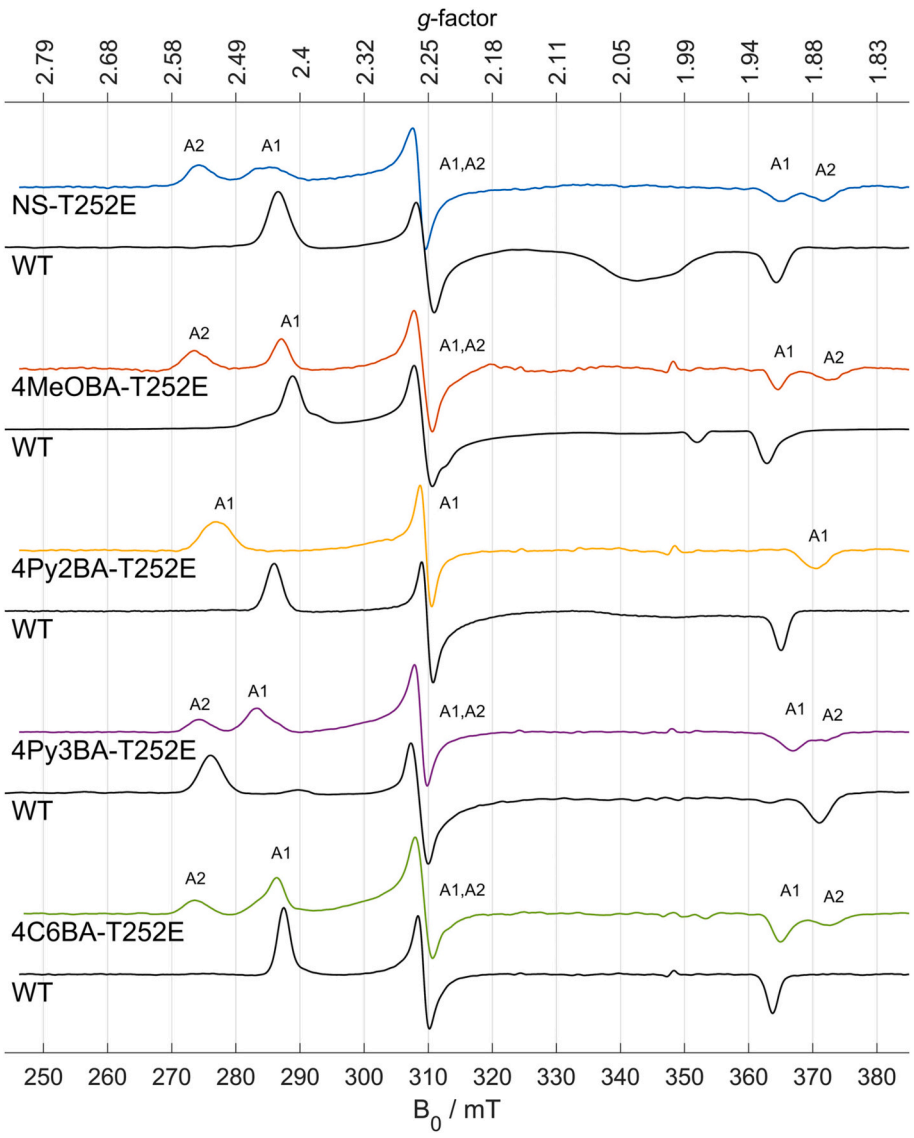

Fig. 4. EPR of the WT and T252E variants of CYP199A4 in the presence of assorted ligands. NS (substrate free), MeOBA (4-methoxybenzoic acid), [59] 4Py2BA (4-pyridin-2-ylbenzoic acid), 4Py3BA (4-pyridin-3-ylbenzoic acid) 4C6BA (4-cyclohexylbenzoic acid). The g-value positions of the components are marked as 'A1' and 'A2'.

crystal structure, and 100% in the 4-thiophen-3-ylbenzoate-T252E structure (Table S8 and S9). The Fe–O distances are 2.3 and 2.1 Å, respectively. In the 4-benzylbenzoate- T252E CYP199A4 structure, the *para*-benzyl group points away from the heme and occupies the space vacated by F298 (Fig. 5). The closest carbon atom of 4-benzylbenzoic acid to the heme iron is the benzylic carbon (4.8 Å), and this is the position at which the substrate is hydroxylated by the CYP199A4 WT and T252E enzymes (Table S8). The *B*-factors are higher for the atoms of the *para*-benzyl group than those of the benzoic acid moiety, indicating that the benzyl group has greater mobility in the active site (Table S10). [92,93]

The overlaid structures of WT CYP199A4 and the T252E mutant in complex with 4-thiophen-3-ylbenzoic acid reveals that the position of the substrate is similar in both structures. The most significant difference was that the water ligand was present in the T252E variant and as a result the substrate appears to be subtly shifted away from the heme in this structure. The thiophene ring of 4-thiophen-3-ylbenzoic acid could either be oriented with the sulfur pointing 'down' towards the heme or pointing 'up' away from the heme (Fig. S22). Both orientations of the ligand were modelled, and the refined occupancies of these alternative conformations were 36% 'down' and 45% 'up' in the T252E structure (Tables S11 and S12); the overall occupancy of the substrate was 81%. In the 'down' orientation the distance between the aqua ligand and sulfur is 4.3 Å (Table S10). An interaction between the sulfur and aqua ligand would explain the 1.0 nm Soret band red-shift induced by this substrate. [94] In the WT structure, the ligand is oriented with the sulfur pointing 'down' towards the heme, and the water is displaced by this bulky ligand. [84]

Although we obtained crystals of the 4-pyridin-3-ylbenzoate- T252E CYP199A4 complex they did not diffract, and we were unable to solve the crystal structure (Fig. S20). The crystal structure of 4-pyridin-2-ylbenzoate-bound T252E CYP199A4, on the other hand, was determined at 1.73-Å resolution (Table S7 and Fig. S19). This crystal structure revealed that the binding mode of 4-pyridin-2-ylbenzoic acid in T252E CYP199A4 is almost identical to its binding mode in WT CYP199A4 (Fig. 7 and Fig. S23). The nitrogen of the pyridine moiety hydrogen-bonds to the heme-bound H_2O/OH^- ligand, the occupancy of which is 100% (Fig. 7, Fig. S24 and Table S13). The Fe–O distance is 2.3 Å and the donor-acceptor distance between the H_2O/OH^- ligand and pyridine N is 2.7 Å. This hydrogen bond is slightly shorter than in the WT enzyme

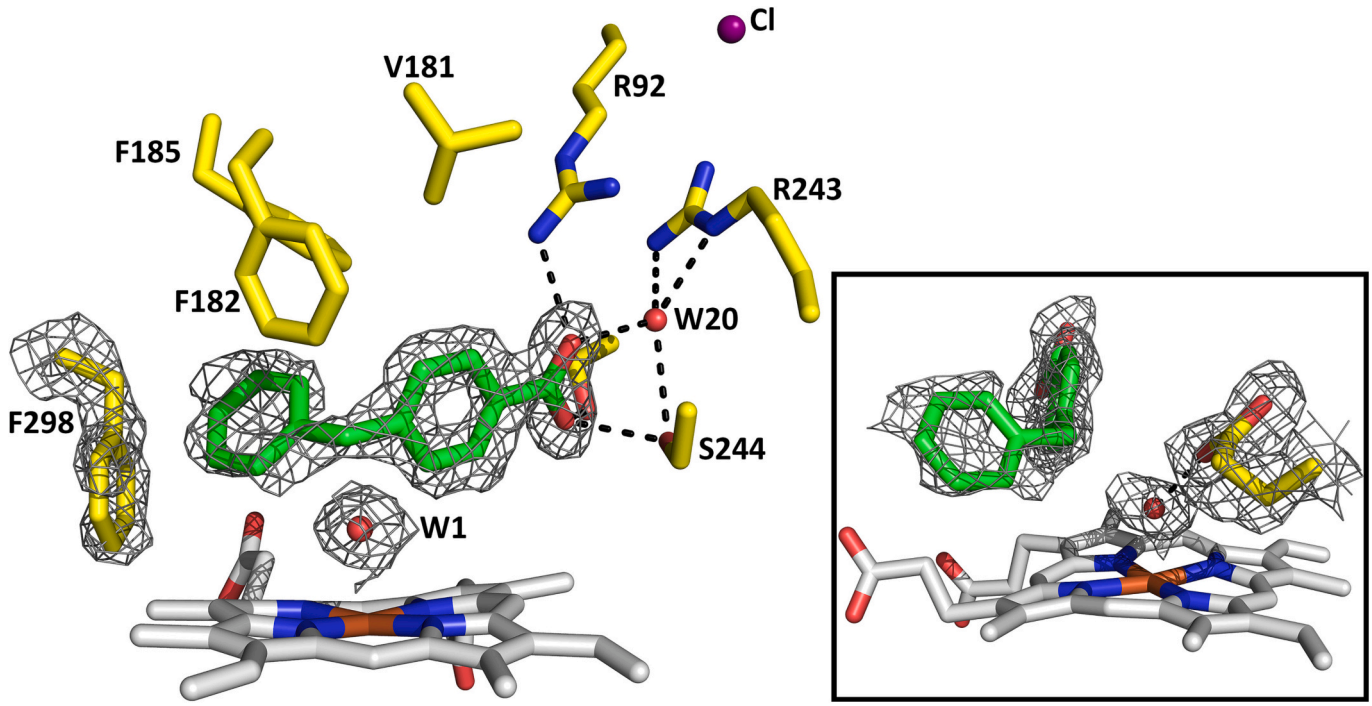

Fig. 5. The crystal structure of the T252E mutant of CYP199A4 in complex with 4-benzylbenzoate determined at 1.79-Å resolution. A $2mF_o$-DF_c **feature-enhanced map** of the substrate, F298 side chain and heme-bound aqua ligand (W1) is shown as grey mesh contoured at 1.0 σ (1.5 Å carve). The image below shows the interaction between the E252 carboxylate and the heme-bound aqua ligand. (For interpretation of the references to colour in this figure legend, the reader is referred to the web version of this article.)

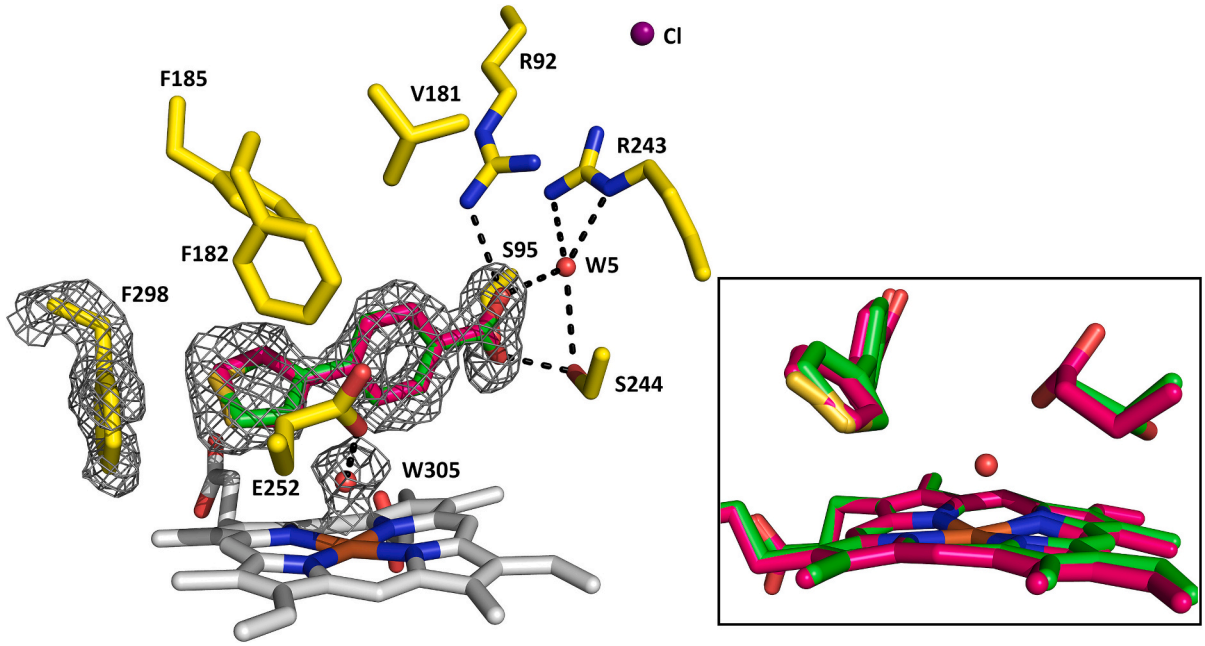

Fig. 6. The crystal structure of the T252E mutant of CYP199A4 in complex with 4-thiophen-3-ylbenzoate. A feature-enhanced map of the substrate, F298, and water ligand (W305) is shown as grey mesh contoured at 1.0 σ (1.5 Å carve). The two orientations of the 4-thiophen-3-ylbenzoic acid ligand are shown in green (sulfur pointing 'up' away from heme) and pink (sulfur pointing 'down' towards heme). Overlaid structures of WT (green; PDB: 6C3J) and T252E CYP199A4 (pink) with 4-thiophen-3-ylbenzoate bound. The waters and chloride in the T252E structure are labelled. (For interpretation of the references to colour in this figure legend, the reader is referred to the web version of this article.)

(2.9 Å; Fig. S23 and Table S13).

In the crystal structures of T252E CYP199A4 in complex with 4-methoxy- and 4-pyridin-2-yl-benzoic acid, the cysteine sulfur ligand, iron and H_2O/OH^- ligand are linearly arranged (S-Fe-O angle ≈180°; Table S13). We noticed that when 4-benzylbenzoic acid and 4-thiophen-3-ylbenzoic acid are bound, the S-Fe-O angle is noticeably bent with the aqua/hydroxo ligand shifted away from the sterically bulky substrate towards the side chain of the glutamate residue (Fig. 8). In the 4-thiophen-3-ylbenzoic acid structure, the Fe–O bond is at a 20.7° angle to the Fe–S bond. In the 4-benzylbenzoic acid structure, the Fe–O bond is at

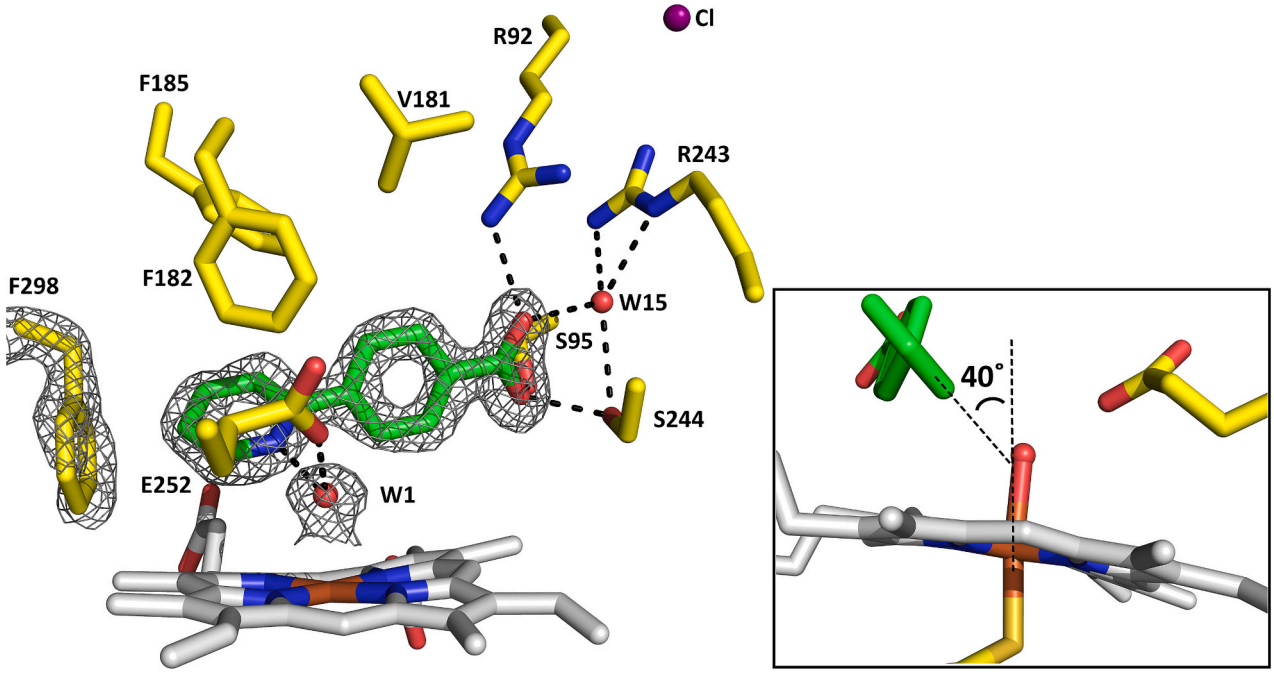

Fig. 7. The crystal structure of the T252E mutant of CYP199A4 in complex with 4-pyridin-2-ylbenzoate. A feature-enhanced map of the substrate, F298, and water ligand (W1) is shown as grey mesh contoured at 2.0 σ (1.5 Å carve). The pyridine ring is at a 40° angle to the Fe–S bond.

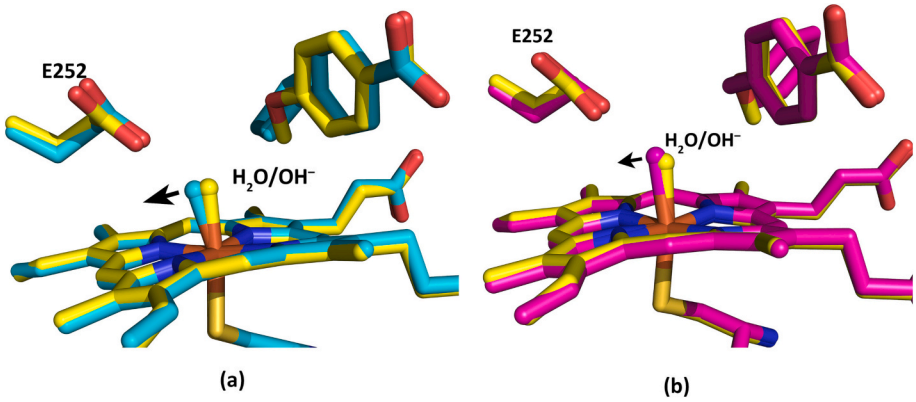

Fig. 8. The active-site structure of 4-methoxybenzoic acid-bound T252E CYP199A4 (yellow) overlaid with **(a)** the 4-thiophen-3-ylbenzoic acid structure (blue) and **(b)** the 4-benzylbenzoic acid structure (magenta). When bulky hydrophobic substrates are bound, the S-Fe-O angle is bent because the H_2O/OH^- ligand is shifted away from the sterically bulky substrate (black arrow). (For interpretation of the references to colour in this figure legend, the reader is referred to the web version of this article.)

a 13.7° angle to the Fe–S bond.

Aside from the differences outlined above the other general features of the heme were consistent with other ferric 6-coordinate species of CYP199A4 (Tables S15 - S19). The iron was more into the plane of the porphyrin ring compared to when the aqua ligand is displaced in the WT enzyme (Fig. S25, Table S15 and S16). The length of the iron-cysteinate sulfur (Fe–S) bond in the T252E variant of CYP199A4 was similar to 6-coordinate type II ligands reported so far with the WT and was marginally shorter than when five coordinate CYP199A4 complexes are formed (Table S17 and S18). The three structures reported here demonstrate differences between the oxygens of the 6th aqua ligand and the glutamate side chain with the shortest being 2.2 Å (4-thiophen-3-ylbenzoic acid) and the longest 2.6 Å (4-methoxybenzoic acid; Table S20). In all structures of the T252E mutant reported here the F298 residue was pushed away from the heme by the larger substrate ligand when compared to the structure of this variant with 4-methoxybenzoic acid. The modified position of F298 was similar to that reported in the crystal structure with 4-ethylthiobenzoic acid. This, and the rotated phenyl ring in the 4-methylthiobenzoic acid crystal structure, demonstrate the flexible nature of the structure of the active site of this enzyme in this region (Fig. S26). [95]

The crystals of CYP199A4 and its mutants are obtained in Bis-Tris buffer between pH 5.0 and 5.75. Given the EPR results, and the changes in the coordination of the 6th aqua ligand described above and the variation in UV–Vis absorbance spectrum of T252E CYP199A4 at lower pH we measured the UV–Vis spectra of this mutant with the other ligands. The biggest change was observed with 4-cyclohexylbenzoic acid where a significant shoulder at ~390 nm was observed at pH 5.5 indicative of the presence of high-spin ferric heme (equivalent to ~40% HS). Smaller changes were with 4-*t*-butylbenzoic acid, 4-benzylbenzoic acid and 4-thiophen-3-ylbenzoic acid but all generated a slightly broader Soret band when compared to that obtained at pH 7.4 (Fig. S27 and Fig. S5). Only minor differences were observed between the spectra obtained for T252E with the pyridinyl ligands at pH 5.5 versus pH 7.4

(Fig. S27 and Fig. 3). However, the Soret band of T252E bound to 4-pyridin-3-yl-benzoic acid was broader than that with 4-pyridin-2-yl-benzoic acid (Fig. S28). The narrow Soret band in the presence of 4-pyridin-2-yl-benzoic acid agrees with the single species observed in the EPR spectrum (Fig. 4). Overall, this suggest that the pH may have a small effect on the heme environment of the T252E variant with the ligand being more loosely bound at lower values. However, the results all demonstrate that this ligand is significantly more difficult to remove in this mutant when compared to the WT enzyme.

4. Conclusions

The T252E mutant of CYP199A4 almost entirely abolishes CYP199A4's ability to utilise NADH/O_2 to oxidise substrates via the normal catalytic cycle. The low activity observed with 4-ethylbenzoic acid confirms this. Although the T252E mutant is unable to efficiently utilise NADH/O_2 to drive catalysis, the peroxygenase activity of CYP199A4 is enhanced by this mutation and it was observed to hydroxylate 4-benzylbenzoic acid using hydrogen peroxide.

This study reveals that even sterically bulky ligands including nitrogen donors are unable to displace the aqua/hydroxo ligand in the T252E mutant, which must be tightly bound. The lack of any significant spin-state shift to HS upon addition of substrates, the exceedingly slow NADH consumption rate and the low coupling efficiency could be explained by the fact that the H_2O/OH^- ligand to the ferric heme is tightly bound and is not displaced by any of the substrates tested here. Crystal structures of the T252E mutant in complex with various other sterically bulky ligands show that the H_2O/OH^- ligand interacts strongly with the side-chain carboxylate of Glu252. The Glu252 carboxylate occupies essentially the same position in all the crystal structures. The closest oxygen of the Glu252 carboxylate is ~4.2 Å from the heme iron. This is closer than the iron-carboxylate distance in chloroperoxidase (5.1 Å). [40] The occupancy of the aqua/hydroxo ligand is close to 100% even when the bulky substrates are bound. Because the iron is six-coordinate and low-spin even when substrate is bound, the iron is predominantly in the plane of the porphyrin ring. In the instances when we were unable to solve complete crystal structures of the T252E mutant in complex with the ligands the UV–Vis spectra demonstrated that the H_2O/OH^- ligand has not been displaced. The EPR data confirmed the low spin nature of the ferric heme in this variant and that at least two heme environments were present under the conditions used for these measurements.

Addition of 4-thiophen-3-yl- and 4-methylthio-benzoic acid to the T252E mutant induced a red-shift of the Soret peak as did the pyridinyl ligands. The sulfur containing ligands induce type I shifts when they bind to WT CYP199A4. [52] These red-shifts may be due to interactions between the sulfur and the sixth axial ligand to the ferric heme in the T252E mutant, which may alter the ligand field strength. [94] The crystal structures reveal that there is an interaction between the sulfur of 4-thiophen-3-ylbenzoic acid and the oxygen ligand in one orientation of the thiophenyl ring.

In summary, we have demonstrated that modification of the active site I-helix threonine residue, which is conserved in most cytochrome P450 enzymes, to a glutamate residue results in a strengthening of the distal aqua ligand in the ferric state. This aqua ligand was not displaced using any of the ligands we tested during this study and explains why this mutant shuts down the monooxygenase activity of the enzyme. Further work to understand why this modification enhances peroxygenase activity is underway.

CRediT authorship contribution statement

Matthew N. Podgorski: Methodology, Formal analysis, Investigation, Visualization, Writing – original draft. **Joel H.Z. Lee:** Methodology, Formal analysis, Investigation, Visualization. **Joshua S. Harbort:** Methodology, Formal analysis, Investigation, Visualization. **Giang T.H. Nguyen:** Methodology, Formal analysis, Investigation, Visualization. **Daniel Z. Doherty:** Methodology, Investigation. **William A. Donald:** Methodology, Formal analysis, Writing – review & editing, Supervision. **Jeffrey R. Harmer:** Methodology, Formal analysis, Writing – review & editing, Supervision. **John B. Bruning:** Formal analysis, Writing – review & editing. **Stephen G. Bell:** Conceptualization, Formal analysis, Writing – original draft, Writing – review & editing, Supervision, Project administration, Funding acquisition.

Declaration of Competing Interest

The authors declare that they have no known competing financial interests or personal relationships that could have appeared to influence the work reported in this paper.

Data availability

The majority if not all of the data used in this manuscript is provided in the document and supplementary material. Other data (if any not available) available up request.

Acknowledgements

This work was supported in part by Australian Research Council (ARC) grants DP140103229 (to S.G.B.), DP200100335 (to J.R.H) and DP160102681 (W.A.D.). S.G.B., J.R.H., and W.A.D. acknowledge the ARC for Future Fellowships (FT140100355, FT120100421, and FT200100798, respectively). The authors also acknowledge the award of an Australian Government Research Training Program Scholarship to M.N.P. (M. Phil), a University of Queensland PhD Scholarship, to J.S.H. and the UNSW for a Tuition Fee Scholarship to G.T.H.N. M.N.P. thanks the University of Adelaide for a Constance Fraser PhD Scholarship and AINSE Ltd. for a Postgraduate Research Award (PGRA). J.H.Z.L. thanks the University of Adelaide for a Constance Fraser PhD Scholarship and the CSIRO Synthetic Biology Future Science Platform for a scholarship. We would like to thank the scientists at the MX1 and MX2 beamline at the Australian Synchrotron for help with data collection. We acknowledge ANSTO for financial support and in providing the facility used in this work. We thank the Bioanalytical Mass Spectrometry Facility and Electron Microscope Unit of the Mark Wainwright Analytical Centre at the UNSW.

Appendix A. Supplementary data

Supplementary data to this article can be found online at https://doi.org/10.1016/j.jinorgbio.2023.112391.

References

[1] M.A. Correia, P.R. Ortiz de Montellano, Inhibition of cytochrome P450 enzymes, in: P.R. Ortiz de Montellano (Ed.), Cytochrome P450: Structure, Mechanism, and Biochemistry, Springer US, Boston, MA, 2005, pp. 247–322.
[2] P.R. Ortiz de Montellano, Hydrocarbon hydroxylation by cytochrome P450 enzymes, Chem. Rev. 110 (2010) 932–948.
[3] D.R. Nelson, Cytochrome P450 diversity in the tree of life, Biochim. Biophys. Acta, Proteins Proteomics 1866 (2018) 141–154.
[4] D.C. Lamb, L. Lei, A.G.S. Warrilow, G.I. Lepesheva, J.G.L. Mullins, M.R. Waterman, S.L. Kelly, The first virally encoded cytochrome P450, J. Virol. 83 (2009) 8266–8269.
[5] E. Plettner, Preface: cytochrome P450, Biochim. Biophys. Acta, Proteins Proteomics 1866 (2018) 1.
[6] F.P. Guengerich, Common and uncommon cytochrome P450 reactions related to metabolism and chemical toxicity, Chem. Res. Toxicol. 14 (2001) 611–650.
[7] R. Oshima, S. Fushinobu, F. Su, L. Zhang, N. Takaya, H. Shoun, Structural evidence for direct hydride transfer from NADH to cytochrome P450nor, J. Mol. Biol. 342 (2004) 207–217.
[8] X. Zhang, S. Li, Expansion of chemical space for natural products by uncommon P450 reactions, Nat. Prod. Rep. 34 (2017) 1061–1089.
[9] P.S. Coelho, E.M. Brustad, A. Kannan, F.H. Arnold, Olefin cyclopropanation via carbene transfer catalyzed by engineered cytochrome P450 enzymes, Science 339 (2013) 307–310.

[10] C.K. Prier, R.K. Zhang, A.R. Buller, S. Brinkmann-Chen, F.H. Arnold, Enantioselective, intermolecular benzylic C–H amination catalysed by an engineered iron-haem enzyme, Nat. Chem. 9 (2017) 629.

[11] C.C. Farwell, J.A. McIntosh, T.K. Hyster, Z.J. Wang, F.H. Arnold, Enantioselective Imidation of sulfides via enzyme-catalyzed intermolecular nitrogen-atom transfer, J. Am. Chem. Soc. 136 (2014) 8766–8771.

[12] C.C. Farwell, R.K. Zhang, J.A. McIntosh, T.K. Hyster, F.H. Arnold, Enantioselective enzyme-catalyzed aziridination enabled by active-site evolution of a cytochrome P450, ACS Cent. Sci. 1 (2015) 89–93.

[13] R. Bernhardt, V.B. Urlacher, Cytochromes P450 as promising catalysts for biotechnological application: chances and limitations, Appl. Microbiol. Biotechnol. 98 (2014) 6185–6203.

[14] X. Wang, T. Saba, H.H.P. Yiu, R.F. Howe, J.A. Anderson, J. Shi, Cofactor NAD(P)H regeneration inspired by heterogeneous pathways, Chem 2 (2017) 621–654.

[15] H. Wu, C. Tian, X. Song, C. Liu, D. Yang, Z. Jiang, Methods for the regeneration of nicotinamide coenzymes, Green Chem. 15 (2013) 1773–1789.

[16] S. Shaik, S. Cohen, Y. Wang, H. Chen, D. Kumar, W. Thiel, P450 enzymes: their structure, reactivity, and selectivity—modeled by QM/MM calculations, Chem. Rev. 110 (2010) 949–1017.

[17] M.J. Honeychurch, H.A.O. Hill, L.-L. Wong, The thermodynamics and kinetics of electron transfer in the cytochrome $P450_{cam}$ enzyme system, FEBS Lett. 451 (1999) 351–353.

[18] D. Correddu, G. Di Nardo, G. Gilardi, Self-sufficient class VII cytochromes P450: from full-length structure to synthetic biology applications, Trends Biotechnol. 39 (2021) 1184–1207.

[19] C.J. Whitehouse, S.G. Bell, L.L. Wong, P450(BM3) (CYP102A1): connecting the dots, Chem. Soc. Rev. 41 (2012) 1218–1260.

[20] S. Nagano, T.L. Poulos, Crystallographic study on the dioxygen complex of wild-type and mutant cytochrome P450cam: implications for the dioxygen activation mechanism, J. Biol. Chem. 280 (2005) 31659–31663.

[21] I. Schlichting, J. Berendzen, K. Chu, A.M. Stock, S.A. Maves, D.E. Benson, R. M. Sweet, D. Ringe, G.A. Petsko, S.G. Sligar, The catalytic pathway of cytochrome P450cam at atomic resolution, Science 287 (2000) 1615–1622.

[22] M. Imai, H. Shimada, Y. Watanabe, Y. Matsushima-Hibiya, R. Makino, H. Koga, T. Horiuchi, Y. Ishimura, Uncoupling of the cytochrome P-450cam monooxygenase reaction by a single mutation, threonine-252 to alanine or valine: possible role of the hydroxy amino acid in oxygen activation, Proc. Natl. Acad. Sci. U. S. A. 86 (1989) 7823–7827.

[23] Y. Kimata, H. Shimada, T. Hirose, Y. Ishimura, Role of THR-252 in cytochrome $P450_{CAM}$: a study with unnatural amino acid mutagenesis, Biochem. Biophys. Res. Commun. 208 (1995) 96–102.

[24] R. Raag, S.A. Martinis, S.G. Sligar, T.L. Poulos, Crystal structure of the cytochrome $P\text{-}450_{CAM}$ active site mutant Thr252Ala, Biochemistry 30 (1991) 11420–11429.

[25] C. Zhang, G. Gilardi, G. Di Nardo, Depicting the proton relay network in human aromatase: new insights into the role of the alcohol-acid pair, Protein Sci. 31 (2022), e4389.

[26] T.L. Poulos, Heme enzyme structure and function, Chem. Rev. 114 (2014) 3919–3962.

[27] M. Vidakovic, S.G. Sligar, H. Li, T.L. Poulos, Understanding the role of the essential Asp251 in cytochrome P450cam using site-directed mutagenesis, crystallography, and kinetic solvent isotope effect, Biochemistry 37 (1998) 9211–9219.

[28] E.G. Hrycay, S.M. Bandiera, Monooxygenase, peroxidase and peroxygenase properties and reaction mechanisms of cytochrome P450 enzymes, in: E.G. Hrycay, S.M. Bandiera (Eds.), Monooxygenase, Peroxidase and Peroxygenase Properties and Mechanisms of Cytochrome P450, Springer International Publishing, Cham, 2015, pp. 1–61.

[29] R. Perera, S. Jin, M. Sono, J.H. Dawson, Cytochrome P450-catalyzed hydroxylations and epoxidations, in: A. Sigel, H. Sigel, R.K. Sigel (Eds.), The Ubiquitous Roles of Cytochrome P450 Proteins, John Wiley & Sons Ltd, Chichester, 2007.

[30] S. Hayakawa, H. Matsumura, N. Nakamura, M. Yohda, H. Ohno, Identification of the rate-limiting step of the peroxygenase reactions catalyzed by the thermophilic cytochrome P450 from *Sulfolobus tokodaii* strain 7, FEBS J. 281 (2014) 1409–1416.

[31] J. Rittle, M.T. Green, Cytochrome P450 compound I: capture, characterization, and C-H bond activation kinetics, Science 330 (2010) 933–937.

[32] J.T. Groves, Key elements of the chemistry of cytochrome P-450: the oxygen rebound mechanism, J. Chem. Educ. 62 (1985) 928.

[33] M.R. Sarkar, S.D. Houston, G.P. Savage, C.M. Williams, E.H. Krenske, S.G. Bell, J. J. De Voss, Rearrangement-free hydroxylation of methylcubanes by a cytochrome P450: the case for dynamical coupling of C-H abstraction and rebound, J. Am. Chem. Soc. 141 (2019) 19688–19699.

[34] N. Raimund, P.R. J, Diverging mechanisms: cytochrome-P450-catalyzed demethylation and γ-lactone formation in bacterial gibberellin biosynthesis, Angew. Chem. Int. Ed. 57 (2018) 6082–6085.

[35] A.R. Modi, J.H. Dawson, Oxidizing intermediates in P450 catalysis: A case for multiple oxidants, in: E.G. Hrycay, S.M. Bandiera (Eds.), Monooxygenase, Peroxidase and Peroxygenase Properties and Mechanisms of Cytochrome P450, Springer International Publishing, Cham, 2015, pp. 63–81.

[36] C.P. Cirino, F.H. Arnold, A self-sufficient peroxide-driven hydroxylation biocatalyst, Angew. Chem. Int. Ed. 42 (2003) 3299–3301.

[37] N. Ma, Z. Chen, J. Chen, J. Chen, C. Wang, H. Zhou, L. Yao, O. Shoji, Y. Watanabe, Z. Cong, Dual-functional small molecules for generating an efficient cytochrome P450BM3 peroxygenase, Angew. Chem. Int. Ed. 57 (2018) 7628–7633.

[38] A.C. Harlington, K.E. Shearwin, S.G. Bell, F. Whelan, Efficient O-demethylation of lignin monoaromatics using the peroxygenase activity of cytochrome P450 enzymes, Chem. Commun. 58 (2022) 13321–13324.

[39] S.J.B. Mallinson, M.M. Machovina, R.L. Silveira, M. Garcia-Borràs, N. Gallup, C. W. Johnson, M.D. Allen, M.S. Skaf, M.F. Crowley, E.L. Neidle, K.N. Houk, G. T. Beckham, J.L. DuBois, J.E. McGeehan, A promiscuous cytochrome P450 aromatic O-demethylase for lignin bioconversion, Nat. Commun. 9 (2018) 2487.

[40] O. Shoji, Y. Watanabe, Peroxygenase reactions catalyzed by cytochromes P450, J. Biol. Inorg. Chem. 19 (2014) 529–539.

[41] X. Huang, J.T. Groves, Oxygen activation and radical transformations in heme proteins and metalloporphyrins, Chem. Rev. 118 (2018) 2491–2553.

[42] P. Jones, H.B. Dunford, The mechanism of compound I formation revisited, J. Inorg. Biochem. 99 (2005) 2292–2298.

[43] E. Derat, S. Shaik, The Poulos−kraut mechanism of compound I formation in horseradish peroxidase:a QM/MM study, J. Phys. Chem. B 110 (2006) 10526–10533.

[44] H. Joo, Z. Lin, F.H. Arnold, Laboratory evolution of peroxide-mediated cytochrome P450 hydroxylation, Nature 399 (1999) 670.

[45] O. Shoji, T. Fujishiro, K. Nishio, Y. Kano, H. Kimoto, S.-C. Chien, H. Onoda, A. Muramatsu, S. Tanaka, A. Hori, H. Sugimoto, Y. Shiro, Y. Watanabe, A substrate-binding-state mimic of H_2O_2-dependent cytochrome P450 produced by one-point mutagenesis and peroxygenation of non-native substrates, Cat. Sci. Technol. 6 (2016) 5806–5811.

[46] Q.-S. Li, J. Ogawa, S. Shimizu, Critical role of the residue size at position 87 in H_2O_2-dependent substrate hydroxylation activity and H_2O_2 inactivation of cytochrome P450BM-3, Biochem. Biophys. Res. Commun. 280 (2001) 1258–1261.

[47] P.C. Cirino, F.H. Arnold, Regioselectivity and activity of cytochrome P450 BM-3 and mutant F87A in reactions driven by hydrogen peroxide, Adv. Synth. Catal. 344 (2002) 932–937.

[48] J. Akter, T.P. Stockdale, S.A. Child, J.H.Z. Lee, J.J. De Voss, S.G. Bell, Selective carbon-hydrogen bond hydroxylation using an engineered cytochrome P450 peroxygenase, J. Inorg. Biochem. 244 (2023) 112209.

[49] S.G. Bell, W. Yang, A.B.H. Tan, R. Zhou, E.O.D. Johnson, A. Zhang, W. Zhou, Z. Rao, L.-L. Wong, The crystal structures of 4-methoxybenzoate bound CYP199A2 and CYP199A4: structural changes on substrate binding and the identification of an anion binding site, Dalton Trans. 41 (2012) 8703–8714.

[50] S.G. Bell, R. Zhou, W. Yang, A.B.H. Tan, A.S. Gentleman, L.-L. Wong, W. Zhou, Investigation of the substrate range of CYP199A4: modification of the partition between hydroxylation and desaturation activities by substrate and protein engineering, Chem. Eur. J. 18 (2012) 16677–16688.

[51] J.C. Miller, J.H.Z. Lee, M.A. McLean, R.R. Chao, I.S.J. Stone, T.L. Pukala, J. B. Bruning, J.J. De Voss, M.A. Schuler, S.G. Sligar, S.G. Bell, Engineering C-C bond cleavage activity into a P450 monooxygenase enzyme, J. Am. Chem. Soc. 145 (2023) 9207–9222.

[52] T. Coleman, S.H. Wong, M.N. Podgorski, J.B. Bruning, J.J. De Voss, S.G. Bell, Cytochrome P450 CYP199A4 from *Rhodopseudomonas palustris* catalyzes heteroatom dealkylations, sulfoxidation, and amide and cyclic hemiacetal formation, ACS Catal. (2018) 5915–5927.

[53] T. Coleman, R.R. Chao, J.B. Bruning, J.J. De Voss, S.G. Bell, CYP199A4 catalyses the efficient demethylation and demethenylation of *para*-substituted benzoic acid derivatives, RSC Adv. 5 (2015) 52007–52018.

[54] J.H.Z. Lee, M.N. Podgorski, M. Moir, A.R. Gee, S.G. Bell, Selective oxidations using a cytochrome P450 enzyme variant driven with surrogate oxygen donors and light, Chem. Eur. J. 28 (2022), e202201366.

[55] R. Nagel, R.J. Peters, Probing the specificity of CYP112 in bacterial gibberellin biosynthesis, Biochem. J. 475 (2018) 2167–2177.

[56] M.R. Waterman, V. Ullrich, R.W. Estabrook, Effect of substrate on the spin state of cytochrome P-450 in hepatic microsomes, Arch. Biochem. Biophys. 155 (1973) 355–360.

[57] M.T. Fisher, S.G. Sligar, Control of heme protein redox potential and reduction rate: linear free energy relation between potential and ferric spin state equilibrium, J. Am. Chem. Soc. 107 (1985) 5018–5019.

[58] S.G. Sligar, I.C. Gunsalus, A thermodynamic model of regulation: modulation of redox equilibria in camphor monoxygenase, Proc. Natl. Acad. Sci. U. S. A. 73 (1976) 1078–1082.

[59] M.N. Podgorski, J.S. Harbort, J.H.Z. Lee, G.T.H. Nguyen, J.B. Bruning, W. A. Donald, P.V. Bernhardt, J.R. Harmer, S.G. Bell, An altered heme environment in an engineered cytochrome P450 enzyme enables the switch from monooxygenase to peroxygenase activity, ACS Catal. 12 (2022) 1614–1625.

[60] M.N. Podgorski, J.S. Harbort, J.H.Z. Lee, G.T.H. Nguyen, J.B. Bruning, W. A. Donald, P.V. Bernhardt, J.R. Harmer, S.G. Bell, An altered heme environment in an engineered cytochrome P450 enzyme enables the switch from monooxygenase to peroxygenase activity, ACS Catal. (2022) 1614–1625.

[61] M.N. Podgorski, T. Coleman, R.R. Chao, J.J. De Voss, J.B. Bruning, S.G. Bell, Investigation of the requirements for efficient and selective cytochrome P450 monooxygenase catalysis across different reactions, J. Inorg. Biochem. 203 (2020) 110913.

[62] N.P. Cowieson, D. Aragao, M. Clift, D.J. Ericsson, C. Gee, S.J. Harrop, N. Mudie, S. Panjikar, J.R. Price, A. Riboldi-Tunnicliffe, R. Williamson, T. Caradoc-Davies, MX1: a bending-magnet crystallography beamline serving both chemical and macromolecular crystallography communities at the Australian Synchrotron, J. Synchrotron Radiat. 22 (2015) 187–190.

[63] D. Aragão, J. Aishima, H. Cherukuvada, R. Clarken, M. Clift, N.P. Cowieson, D. J. Ericsson, C.L. Gee, S. Macedo, N. Mudie, S. Panjikar, J.R. Price, A. Riboldi-Tunnicliffe, R. Rostan, R. Williamson, T.T. Caradoc-Davies, MX2: a high-flux undulator microfocus beamline serving both the chemical and macromolecular crystallography communities at the Australian Synchrotron, J. Synchrotron Radiat. 25 (2018) 885–891.

[64] T.G.G. Battye, L. Kontogiannis, O. Johnson, H.R. Powell, A.G.W. Leslie, iMOSFLM: a new graphical interface for diffraction-image processing with MOSFLM, Acta Crystallogr. D Biol. Crystallogr. 67 (2011) 271–281.
[65] M.D. Winn, C.C. Ballard, K.D. Cowtan, E.J. Dodson, P. Emsley, P.R. Evans, R. M. Keegan, E.B. Krissinel, A.G.W. Leslie, A. McCoy, S.J. McNicholas, G. N. Murshudov, N.S. Pannu, E.A. Potterton, H.R. Powell, R.J. Read, A. Vagin, K. S. Wilson, Overview of the CCP4 suite and current developments, Acta Crystallogr. D Biol. Crystallogr. 67 (2011) 235–242.
[66] P. Legrand, XDSme, undated, https://code.google.com/p/xdsme/.
[67] P.R. Evans, G.N. Murshudov, How good are my data and what is the resolution? Acta Crystallogr. D Biol. Crystallogr. 69 (2013) 1204–1214.
[68] A.J. McCoy, R.W. Grosse-Kunstleve, P.D. Adams, M.D. Winn, L.C. Storoni, R. J. Read, Phaser crystallographic software, J. Appl. Crystallogr. 40 (2007) 658–674.
[69] N.W. Moriarty, R.W. Grosse-Kunstleve, P.D. Adams, Electronic Ligand Builder and Optimization Workbench (eLBOW): a tool for ligand coordinate and restraint generation, Acta Crystallogr. D Biol. Crystallogr. 65 (2009) 1074–1080.
[70] P. Emsley, B. Lohkamp, W.G. Scott, K. Cowtan, Features and development of coot, Acta Crystallogr. D Biol. Crystallogr. 66 (2010) 486–501.
[71] P.V. Afonine, R.W. Grosse-Kunstleve, N. Echols, J.J. Headd, N.W. Moriarty, M. Mustyakimov, T.C. Terwilliger, A. Urzhumtsev, P.H. Zwart, P.D. Adams, Towards automated crystallographic structure refinement with phenix.refine, Acta Crystallogr. D Biol. Crystallogr 68 (2012) 352–367.
[72] V.B. Chen, W.B. Arendall III, J.J. Headd, D.A. Keedy, R.M. Immormino, G.J. Kapral, L.W. Murray, J.S. Richardson, D.C. Richardson, MolProbity: all-atom structure validation for macromolecular crystallography, Acta Crystallogr. D Biol. Crystallogr. 66 (2010) 12–21.
[73] P.D. Adams, P.V. Afonine, G. Bunkoczi, V.B. Chen, I.W. Davis, N. Echols, J. J. Headd, L.-W. Hung, G.J. Kapral, R.W. Grosse-Kunstleve, A.J. McCoy, N. W. Moriarty, R. Oeffner, R.J. Read, D.C. Richardson, J.S. Richardson, T. C. Terwilliger, P.H. Zwart, PHENIX: a comprehensive Python-based system for macromolecular structure solution, Acta Crystallogr. D Biol. Crystallogr. 66 (2010) 213–221.
[74] P.V. Afonine, N.W. Moriarty, M. Mustyakimov, O.V. Sobolev, T.C. Terwilliger, D. Turk, A. Urzhumtsev, P.D. Adams, FEM: feature-enhanced map, Acta Crystallogr. D Biol. Crystallogr. 71 (2015) 646–666.
[75] T.C. Terwilliger, R.W. Grosse-Kunstleve, P.V. Afonine, N.W. Moriarty, P.D. Adams, R.J. Read, P.H. Zwart, L.-W. Hung, Iterative-build OMIT maps: map improvement by iterative model building and refinement without model bias, Acta Crystallogr. D Biol. Crystallogr. 64 (2008) 515–524.
[76] L.L.C. Schrodinger, The PyMOL Molecular Graphics System, Version 1.4.1, 2015.
[77] G.T.H. Nguyen, T.N. Tran, M.N. Podgorski, S.G. Bell, C.T. Supuran, W.A. Donald, Nanoscale ion emitters in native mass spectrometry for measuring ligand–protein binding affinities, ACS Cent. Sci. 5 (2019) 308–318.
[78] M.N. Podgorski, J.S. Harbort, T. Coleman, J.E. Stok, J.A. Yorke, L.-L. Wong, J. B. Bruning, P.V. Bernhardt, J.J. De Voss, J.R. Harmer, S.G. Bell, Biophysical techniques for distinguishing ligand binding modes in cytochrome P450 monooxygenases, Biochemistry 59 (2020) 1038–1050.
[79] H.M. Girvan, H.E. Seward, H.S. Toogood, M.R. Cheesman, D. Leys, A.W. Munro, Structural and spectroscopic characterization of P450 BM3 mutants with unprecedented P450 heme iron ligand sets: new heme ligation states influence conformational equilibria in P450 BM3, J. Biol. Chem. 282 (2007) 564–572.
[80] T. Coleman, R.R. Chao, J.J. De Voss, S.G. Bell, The importance of the benzoic acid carboxylate moiety for substrate recognition by CYP199A4 from *Rhodopseudomonas palustris* HaA2, Biochim. Biophys. Acta, Proteins Proteomics 1864 (2016) 667–675.
[81] J.L. Bennett, G.T.H. Nguyen, W.A. Donald, Protein-small molecule interactions in native mass spectrometry, Chem. Rev. 122 (2022) 7327–7385.
[82] G.T.H. Nguyen, J.L. Bennett, S. Liu, S.E. Hancock, D.L. Winter, D.J. Glover, W. A. Donald, Multiplexed screening of thousands of natural products for protein-ligand binding in native mass spectrometry, J. Am. Chem. Soc. 143 (2021) 21379–21387.
[83] T. Coleman, J.Z.H. Lee, A.M. Kirk, D.Z. Doherty, M.N. Podgorski, D.K. Pinidiya, J. B. Bruning, J.J. De Voss, E.H. Krenske, S.G. Bell, Enabling aromatic hydroxylation in a cytochrome P450 monooxygenase enzyme through protein engineering, Chem. Eur. J. 28 (2022), e202201895.
[84] M.N. Podgorski, A.B. Keto, T. Coleman, J.B. Bruning, J.J. De Voss, E.H. Krenske, S. G. Bell, The oxidation of oxygen and sulfur-containing heterocycles by cytochrome P450 enzymes, Chem. Eur. J. 50 (2023), e202301371.
[85] T. Coleman, A.M. Kirk, J.H.Z. Lee, D.Z. Doherty, J.B. Bruning, E.H. Krenske, J.J. De Voss, S.G. Bell, Different geometric requirements for cytochrome P450-catalyzed aliphatic versus aromatic hydroxylation results in chemoselective oxidation, ACS Catal. 12 (2022) 1258–1267.
[86] J.H. Dawson, L.A. Andersson, M. Sono, Spectroscopic investigations of ferric cytochrome P-450-CAM ligand complexes. Identification of the ligand *trans* to cysteinate in the native enzyme, J. Biol. Chem. 257 (1982) 3606–3617.
[87] Y. Yoshida, Y. Aoyama, T. Nishino, H. Katsuki, U.S. Maitra, V.P. Mohan, D. B. Sprinson, Spectral properties of a novel cytochrome P-450 of a *Saccharomyces cerevisiae* mutant SG1. A cytochrome P-450 species having a nitrogenous ligand *trans* to thiolate, Biochem. Biophys. Res. Commun. 127 (1985) 623–628.
[88] J.H. Dawson, L.A. Andersson, M. Sono, The diverse spectroscopic properties of ferrous cytochrome P-450-CAM ligand complexes, J. Biol. Chem. 258 (1983) 13637–13645.
[89] A. Famulari, D. Correddu, G. Di Nardo, G. Gilardi, M. Chiesa, I. García-Rubio, EPR characterization of the heme domain of a self-sufficient cytochrome P450 (CYP116B5), J. Inorg. Biochem. 231 (2022) 111785.
[90] T. Jovanovic, R. Farid, R.A. Friesner, A.E. McDermott, Thermal equilibrium of high- and low-spin forms of cytochrome P450 BM-3: repositioning of the substrate? J. Am. Chem. Soc. 127 (2005) 13548–13552.
[91] R.J. Lawson, D. Leys, M.J. Sutcliffe, C.A. Kemp, M.R. Cheesman, S.J. Smith, J. Clarkson, W.E. Smith, I. Haq, J.B. Perkins, A.W. Munro, Thermodynamic and biophysical characterization of cytochrome P450 BioI from Bacillus subtilis, Biochemistry 43 (2004) 12410–12426.
[92] J.-M. Rondeau, H. Schreuder, Protein Crystallography and Drug Discovery, The Practice of Medicinal Chemistry (Third Edition), Academic Press, New York, 2008, pp. 605–634.
[93] A. Wlodawer, W. Minor, Z. Dauter, M. Jaskolski, Protein crystallography for non-crystallographers, or how to get the best (but not more) from published macromolecular structures, FEBS J. 275 (2008) 1–21.
[94] K.P. Conner, P. Vennam, C.M. Woods, M.D. Krzyaniak, M.K. Bowman, W.M. Atkins, 1,2,3-triazole–heme interactions in cytochrome P450: functionally competent triazole–water–heme complexes, Biochemistry 51 (2012) 6441–6457.
[95] M.N. Podgorski, T. Coleman, L.R. Churchman, J.B. Bruning, J.J. De Voss, S.G. Bell, Investigating the active oxidants involved in cytochrome P450 catalyzed sulfoxidation reactions, Chem. Eur. J. 28 (2022), e202202428.